

Phase transition in time-reversible Navier-Stokes equations

Vishwanath Shukla^{1,2,3,*}, Bérengère Dubrulle⁴, Sergey Nazarenko³, Giorgio Krstulovic⁵ and Simon Thalabard⁶

¹Department of Physics, Indian Institute of Technology Kharagpur, Kharagpur 721302, India

²Centre for Theoretical Studies, Indian Institute of Technology Kharagpur, Kharagpur-721302, India

³Université Côte d'Azur, Institut de Physique de Nice (INPHYNI), CNRS UMR 7010, Parc Valrose, 06108 Nice Cedex 2, France

⁴DSM/IRAMIS/SPEC, CNRS UMR 3680, CEA, Université Paris-Saclay, 91190 Gif sur Yvette, France

⁵Université Côte d'Azur, CNRS, OCA, Laboratoire Lagrange, Bd. de l'Observatoire, 06300 Nice, France

⁶Instituto Nacional de Matemática Pura e Aplicada, IMPA, 22460-320 Rio de Janeiro, Brazil



(Received 28 November 2018; revised manuscript received 20 July 2019; published 9 October 2019)

We present a comprehensive study of the statistical features of a three-dimensional (3D) time-reversible truncated Navier-Stokes (RNS) system, wherein the standard viscosity ν is replaced by a fluctuating thermostat that dynamically compensates for fluctuations in the total energy. We analyze the statistical features of the RNS steady states in terms of a non-negative dimensionless control parameter \mathcal{R}_r , which quantifies the balance between the fluctuations of kinetic energy at the forcing length scale ℓ_f and the total energy E_0 . For small \mathcal{R}_r , the RNS equations are found to produce “warm” stationary statistics, e.g., characterized by the partial thermalization of the small scales. For large \mathcal{R}_r , the stationary solutions have features akin to standard hydrodynamic ones: they have compact energy support in k space and are essentially insensitive to the truncation scale k_{\max} . The transition between the two statistical regimes is observed to be smooth but rather sharp. Using insights from a diffusion model of turbulence (Leith model), we argue that the transition is in fact akin to a *continuous second-order phase transition*, where \mathcal{R}_r indeed behaves as a thermodynamic control parameter, e.g., a temperature. A relevant order parameter can be suitably defined in terms of a (normalized) enstrophy, while the symmetry-breaking parameter h is identified as (one over) the truncation scale k_{\max} . We find that the signatures of the phase transition close to the critical point \mathcal{R}_r^* can essentially be deduced from a heuristic mean-field Landau free energy. This point of view allows us to reinterpret the relevant asymptotics in which the *dynamical ensemble equivalence* conjectured by Gallavotti [Phys. Lett. A **223**, 91 (1996)] could hold true. We argue that Gallavotti’s limit is precisely the joint limit $\mathcal{R}_r \gtrsim \mathcal{R}_r^*$ and $h \gtrsim 0$, with the overset symbol “ \gtrsim ” indicating that those limits are approached from above. The limit therefore relates to the statistical features at the critical point. In this regime, our numerics indicate that the low-order statistics of the 3D RNS are indeed qualitatively similar to those observed in direct numerical simulations of the standard Navier-Stokes equations with viscosity chosen so as to match the average value of the reversible thermostat. This result suggests that Gallavotti’s *equivalence conjecture* could indeed be of relevance to model 3D turbulent statistics, and provides a clear guideline for further numerical investigations involving higher resolutions.

DOI: [10.1103/PhysRevE.100.043104](https://doi.org/10.1103/PhysRevE.100.043104)

I. INTRODUCTION

Describing the irreversible behaviors of macroscopic observables arising from time-reversible microscopic dynamics is the central long-standing theme of nonequilibrium statistical mechanics [1–3]. When there exists a wide scale separation between the microscopic and the macroscopic scales, the emergence of irreversibility can in general be formalized using a variety of reduction techniques including but not limited to stochastic equations, diffusion, or projection operators formalisms that model the collective evolution of the fastest variables [4–7]. In general though, and although the scopes of many promising strategies are the subject of intense research activity [8–12], no systematic framework exists that would allow to derive from first principles a

nonequilibrium thermodynamic formalism that could simply account for macroscopic irreversibility.

In the context of three-dimensional (3D) stationary homogeneous isotropic turbulence, whose statistics stem from standard Navier-Stokes (NS) equations, a hallmark of irreversibility is the phenomenon of anomalous dissipation, namely, the fact that the rate of energy dissipation ϵ becomes finite as the separation between the injection and the dissipative viscous scales become infinite. The breaking of detailed balance is then made apparent through the celebrated four-fifth law (see, e.g. Ref. [13]), which ties ϵ to the average of the cube of the longitudinal velocity increments. This is an anomalous feature, as in the limit of vanishing viscosity (infinite Reynolds number) the flow could in principle formally be described by the time-symmetric Euler equations.

A thorough description of irreversibility in turbulence requires to underpin its precise features and in recent years this problem has witnessed a renewed interest. In particular, nontrivial signatures of irreversibility have been identified on

*research.vishwanath@gmail.com

the Lagrangian statistics: both experiments and large numerical simulations have demonstrated that these depend on the forward-in-time or backward-in-time conditioning [14–17]. For instance, both fluid and heavy particles tend to gain kinetic energy slowly but lose it rapidly along their Lagrangian trajectories [18–20]: This is a clear example of an irreversible behavior, whose origin relates to vortex stretching and generation of small length scales [21], and which persists even in the limit of vanishing viscosity.

One important difficulty in studying turbulent irreversibility precisely comes from its asymptotic nature. Even massive computational effort in numerically integrating the NS equations may fail in clearly disentangling the finite-Reynolds-number effects from the truly asymptotic features [22,23].

An alternative approach is to tweak the governing equations to make them time reversible, and then study whether the irreversible signatures of turbulence still emerge under suitably defined limits. An early example of such dynamics is that of the “constrained Euler system” considered in Ref. [24], wherein the energies contained within narrow wave number shells are held constant in time. The resulting system was shown to reproduce many among the standard statistical features of isotropic turbulence, including intermittency.

In Ref. [25], another time-reversible governing equation was proposed, based on the assumption that the fluid is not subjected to the usual viscous dissipation, but rather to a modified dissipation mechanism, namely, a “reversible viscosity” that balances exactly the injection statistics, and tuned so that a prescribed macroscopic observable such as the total energy or the total enstrophy remains constant in time. This modification transforms the “dissipative term” into a “thermostatting term” which is time-reversal invariant. An equivalence between such above reversible formulations and the standard NS dynamics was postulated to hold true in the limit of high Reynolds number [25], as a consequence of a more general *equivalence of dynamical ensembles* for nonequilibrium systems [26]. Should such an “equivalence conjecture” hold true, at least for suitable choices of thermostat, one would therefore expect that both standard and reversible dynamics could produce the same statistics for inertial range dynamics at finite Reynolds number, provided that both the standard and the averaged reversible viscosity share the same value.

The use of the reversible formulation opens up the possibility to explore the implications of the chaotic hypothesis [27] for the fluctuations of the local observables and the Lyapunov spectrum. This perspective has motivated many investigations, including numerical [28–31] and experimental ones [32].

Numerical tests probing equivalence of dynamical ensembles were performed in various settings but so far and to the best of our knowledge only for models more simple than the full three-dimensional (3D) NS equations. For instance, time-reversible versions of shell models of turbulence obtained by imposing a global constraint of energy conservation were investigated in [28]. It was demonstrated that as the amplitude of the external force is varied, from zero to high values, the system exhibits a smooth transition from an equilibrium state to a nonequilibrium stationary state with an energy cascade from large to small scales.

Such models have also been studied in combination with various kinds of thermostats. Recent results suggest that the relevance of the equivalence conjecture might crucially depend on which macroscopic observable is chosen to be held constant [33,34]. Insights on how macroscopic irreversibility ties to nonequilibrium energy cascade process rather than to the explicit breaking of the time-reversal invariance due to viscous dissipation were also reported in Ref. [35].

The validity of the equivalence conjecture along with various consequences of the chaotic hypothesis were tested for incompressible two-dimensional (2D) flows [29,31]. Direct numerical simulations (DNS) of the incompressible 2D NS equations were compared to their reversible counterpart, in order to examine the fluctuations of global quadratic quantities in statistically stationary states. Comparative study of the Lyapunov spectra showed that they overlapped [31], and this feature provides support in favor of the equivalence conjecture.

The discussion above suggests that suitably defined reversible Navier-Stokes (RNS) systems could perhaps provide a thermodynamic framework, within which genuine turbulent statistics would emerge out of a time-reversible dynamics. This could help at shedding a thermodynamic perspective on typical anomalous turbulent signatures. To that end, the recent works [33,35] constitute very promising steps toward both a systematic assessment and a comprehensive understanding of Gallavotti’s conjecture. To our knowledge, though, no systematic attempt was made so far in order to clearly target the limit in which the equivalence conjecture could supposedly hold true, e.g., the limit $\nu \rightarrow 0$ for the *full* 3D NS equations. The obvious reason for this is the fact that this question is both subtle and *a priori* heavy to tackle from a numerical perspective. Any numerical scheme involves a cutoff scale k_{\max} , and the desired asymptotics is then necessarily a joint limit $k_{\max} \rightarrow \infty$, $\nu \rightarrow 0$. In principle, those two limits do not commute. In the context of Gallavotti’s original equivalence conjecture, one should clearly let $k_{\max} \rightarrow \infty$ before letting $\nu \rightarrow 0$, and in our view even a phenomenological hint as to whether the equivalence conjecture should reasonably hold in that limit is perhaps currently lacking. To gain such an intuition, one should probably first understand the nature of the statistical regimes that the RNS dynamics is likely to generate. Yet, systematic overviews are to this day at best essentially qualitative or simply lack, such is the case for the 3D RNS. This paper intends to fill this gap.

Our work offers a comprehensive study of the statistical features of a 3D time-reversible NS system, in which the standard viscosity is replaced by a fluctuating thermostat that dynamically compensates for fluctuations in the total energy. To identify different statistical regimes of this system, we introduce the non-negative dimensionless control parameter $\mathcal{R}_r = f_0 \ell_f / E_0$, which quantifies the balance between the injection of kinetic energy at the forcing scale ℓ_f and the total energy E_0 . For small values of \mathcal{R}_r , the RNS equations are found to produce steady states which are characterized by close-to-equilibrium Gibbs-type statistics for the small scales. As such, and extending a terminology introduced in [36], we refer to this type of solutions as being *warm*. The terminology is simply meant to convey the idea that the spectra being partially thermalized at the ultraviolet end, the latter should

behave somewhat akin to a heat bath, a feature previously observed in truncated fluid models [37–39]. For large \mathcal{R}_r , the stationary solutions have compact energy support in k space and are found to be essentially insensitive to the cutoff scale k_{\max} (later precisely defined) and we refer to those kind of states as being of *hydrodynamic* type. The transition between the two statistical regimes is observed to be rather sharp. Using insights from a reversible nonlinear diffusion model of turbulence (Leith model), we argue that the transition is in fact akin to a *continuous second-order phase transition*, and that \mathcal{R}_r indeed behaves as a thermodynamic control parameter, e.g., a temperature. A relevant order parameter can be suitably defined in terms of a (normalized) enstrophy, while the symmetry-breaking parameter h is identified as (one over) the truncation scale k_{\max} . We find that the signatures of the phase transition close to the critical point \mathcal{R}_r^* can essentially be deduced from a heuristic mean-field Landau free energy. This point of view allows us to reinterpret the relevant asymptotics in which Gallavotti’s conjecture could hold true. Gallavotti’s limit precisely corresponds to the joint limit $\mathcal{R}_r \xrightarrow{>} \mathcal{R}_r^*$ and $h \xrightarrow{>} 0$, with overset “ $>$ ” meaning that the critical point is approached from above. It therefore relates to the statistics in the neighborhood of the critical point. In this regime, our numerics indicate that the 3D RNS steady statistics mimic their standard NS counterpart, with viscosity matching the average value of the reversible thermostat. This result hints toward the validity of the equivalence conjecture.

The remainder of this paper is organized as follows. Section II introduces the RNS equations and the control parameter \mathcal{R}_r . We schematically discuss the expected statistical features of the RNS states in the two opposite asymptotics $\mathcal{R}_r \rightarrow 0$ and $\mathcal{R}_r \rightarrow \infty$. Section III describes the outcomes of our RNS numerics, and presents a detailed overview of the different statistical regimes which we observe. We identify a small crossover range of \mathcal{R}_r , wherein the RNS states continuously transit from being “warm” to being “hydrodynamic.” Section IV discusses insights obtained from the analysis of a suitably defined “reversible Leith model,” the statistical regimes of which are interpreted within the framework of a mean-field second-order Landau theory. Section V extends the discussion back to the RNS system, and reformulates the equivalence in a thermodynamic framework. We compare low-order RNS and NS statistics slightly above the candidate critical point, and argue that this is indeed the relevant regime to consider. Section VI summarizes our findings and presents some perspectives.

II. REVERSIBLE NAVIER-STOKES EQUATIONS

A. Formal definitions

The spatiotemporal evolution of the velocity field $\mathbf{u}(\mathbf{x}, t)$ describing an incompressible fluid flow within a spatial domain \mathcal{D} is governed by the Navier-Stokes (NS) equations

$$\frac{\partial \mathbf{u}}{\partial t} + (\mathbf{u} \cdot \nabla) \mathbf{u} = -\nabla p + \nu \nabla^2 \mathbf{u} + \mathbf{f}, \quad (1)$$

where ν is the kinematic viscosity, p is the pressure field, and \mathbf{f} is the forcing term, acting at large scales, to sustain a statistically steady state. The incompressibility is ensured by requiring $\nabla \cdot \mathbf{u} = 0$ and the fluid density is set to 1.

In presence of the viscous dissipation term $\nu \nabla^2 \mathbf{u}$, the resulting macroscopic dynamics is clearly irreversible, as the NS equations (1) are not invariant under the transformation

$$\mathcal{T} : t \rightarrow -t; \mathbf{u} \rightarrow -\mathbf{u}. \quad (2)$$

We now follow Ref. [25], and alter the dissipation operator term to make it invariant under the transformation \mathcal{T} . The essential tweak consists in transforming the dissipation operator into a thermostat, so that a certain macroscopic quantity, such as the total energy or the total enstrophy, becomes a conserved quantity. While Ref. [40] discusses several implementations of this idea, we here choose to follow Ref. [28,29], and impose a constraint on the total kinetic energy. An elementary calculation shows that in order for the energy to be held constant, the viscosity must fluctuate as

$$\nu_r[\mathbf{u}] = \frac{\int_{\mathcal{D}} \mathbf{f} \cdot \mathbf{u} \, d\mathbf{x}}{\int_{\mathcal{D}} (\nabla \times \mathbf{u})^2 \, d\mathbf{x}}. \quad (3)$$

This *reversible viscosity* is a functional of \mathbf{u} and depends on the state of the system. We refer to the equations obtained by replacing the constant in time viscosity ν in the NS equations (1) with the state dependent ν_r as the “reversible Navier-Stokes” (RNS) equations:

$$\frac{\partial \mathbf{u}}{\partial t} + (\mathbf{u} \cdot \nabla) \mathbf{u} = -\nabla p + \nu_r \nabla^2 \mathbf{u} + \mathbf{f}, \quad (4)$$

where we still enforce incompressibility as $\nabla \cdot \mathbf{u} = 0$.

B. Reversible control parameter \mathcal{R}_r

To characterize the statistical steady states of the RNS system, we use the dimensionless control parameter

$$\mathcal{R}_r = \frac{f_0 \ell_f}{E_0}, \quad (5)$$

where E_0 is the total (conserved) energy fixed by the initial state, f_0 is the forcing amplitude, and ℓ_f is the energy injection length scale.

Despite its suggestive name, the control parameter \mathcal{R}_r should not be interpreted as either a “reversible Reynolds number” or an inverse thereof: neither of the asymptotic regimes $\mathcal{R}_r \rightarrow 0$ and $\mathcal{R}_r \rightarrow \infty$ does indeed describe a fully developed turbulent state.

This is perhaps slightly counterintuitive as when $\mathcal{R}_r \rightarrow 0$ the RNS dynamics formally reduces to the freely evolving Euler equations. There is yet no reason to expect this limit to produce a “fully developed turbulent” steady state, as it corresponds to a very specific *joint limit*, where both the viscous and the forcing term simultaneously vanish. Fully developed turbulence is in principle generated from the NS equations in a different manner, that is by letting the standard viscosity $\nu \rightarrow 0$ at fixed value of the forcing f_0 [13]. There is therefore no reason that both limits coincide.

This work relies on numerical integrations of the RNS equations. As such, the fact that the limit $\mathcal{R}_r \rightarrow 0$ should be unrelated to turbulence becomes even clearer. Indeed, any numerical calculation involves a finite resolution or equivalently a finite number of degrees of freedom. At fixed resolution, the limit $\mathcal{R}_r \rightarrow 0$ does not yield the Euler equations but rather their *truncated* counterpart. Hence, the numerical integrations

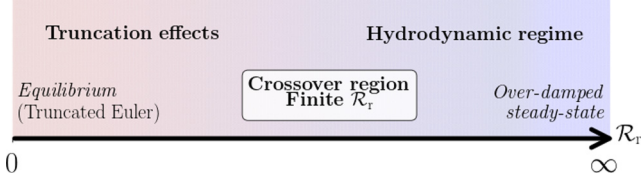


FIG. 1. A schematic illustration of a candidate (truncated) RNS phase diagram with two distinct regimes and a crossover region, that would be compatible with the heuristic description of Sec. II B for the limits $\mathcal{R}_r \rightarrow 0$ and $\mathcal{R}_r \rightarrow \infty$.

of the truncated RNS equations will in the limit $\mathcal{R}_r \rightarrow 0$ converge toward an *absolute equilibrium equipartition state*, describing statistical energy equipartition among the modes. This equilibrium state has Gaussian statistics and does not tie to fully developed turbulence. We refer the reader to Appendix for further details on absolute equilibria and truncated Euler flows.

By contrast, the limit $\mathcal{R}_r \rightarrow \infty$ resembles an overdamped dynamics: in this limit, the forcing is infinitely large compared to the energy retained in the system. Therefore, any energy injected at scale ℓ_f should in principle immediately be removed by the reversible viscosity, hereby suppressing the nonlinear transfer of energy. As such, the asymptotic steady state cannot be sensitive to the number of modes used in the numerical simulations.

The two asymptotic phases should obviously cross over at intermediate values of \mathcal{R}_r , and this is very schematically summarized by the diagram sketched in Fig. 1. Our numerical simulations intend to substantiate this crude phenomenological overview, and in particular provide a detailed characterization of the RNS statistical regimes when \mathcal{R}_r takes a finite value.

III. NUMERICAL EXPERIMENTS

We begin this section with a brief overview of our numerical methods, followed by a comprehensive description of the results obtained from the numerical simulations of the RNS equations. We show that the phase diagram depicted in Fig. 1 is essentially correct. The RNS system indeed has two distinct statistical regimes separated by a crossover region. The transition between these two regimes has the character of a continuous-phase transition.

A. Details of the simulations

1. Numerical schemes

In order to perform the numerical integrations of either the 3D NS [Eq. (1)] or the 3D RNS [Eq. (4)], we use the VIKSHOBHA solver, which is an efficient parallel numerical code, that relies on a highly accurate pseudospectral method [41].

The velocity field \mathbf{u} is solved inside a cubic domain \mathcal{D} of side 2π , and is prescribed to be triply periodic. As such, it is represented by the Fourier series

$$\mathbf{u}(\mathbf{x}, t) = \sum_{\mathbf{k}} \hat{\mathbf{u}}(\mathbf{k}, t) \exp(i\mathbf{k} \cdot \mathbf{x}),$$

where $\mathbf{k} = (k_1, k_2, k_3)$, $k_i \in [-N_c/2, N_c/2 - 1]$ represent the 3D wave numbers and N_c is the number of collocation points. From the incompressibility condition, the pressure term is eliminated by using the transverse projection operator $\mathbb{P}_{i,j}(\mathbf{k}) = \delta_{i,j} - k_i k_j / k^2$, hereby projecting the nonlinear term $\mathbf{u} \cdot \nabla \mathbf{u}$ onto a plane perpendicular to \mathbf{k} . Our pseudospectral method computes the linear terms in Fourier space and the nonlinear terms in real space, before transforming them back to Fourier space. Aliasing errors are removed using the standard $\frac{2}{3}$ -dealiasing rule, so that the maximum wave number in our simulations has magnitude $k_{\max} = N_c/3$. Both the NS and the RNS dynamics are evolved in time using a second-order Runge-Kutta scheme.

In our RNS numerics, the time step was kept very small $dt = 7.5 \times 10^{-4}$, and this allowed very accurate conservation of the energy. Variations are below 0.03% in every one of our runs.

2. Initial data and forcing

Both RNS and DNS runs are initiated from the following Taylor-Green velocity field:

$$\begin{aligned} u_x &= u_0 \sin(x) \cos(y) \cos(z), \\ u_y &= -u_0 \cos(x) \sin(y) \cos(z), \\ u_z &= 0, \end{aligned}$$

and the coefficient u_0 sets the value of the initial energy.

Energy is then injected in the system using the Taylor-Green forcing:

$$\begin{aligned} f_x &= f_0 \sin(\tilde{k}_f x) \cos(\tilde{k}_f y) \cos(\tilde{k}_f z), \\ f_y &= -f_0 \cos(\tilde{k}_f x) \sin(\tilde{k}_f y) \cos(\tilde{k}_f z), \\ f_z &= 0, \end{aligned}$$

where f_0 and \tilde{k}_f are, respectively, the forcing amplitude and wave number. We write $k_f := \sqrt{3}\tilde{k}_f$ as the norm of the forcing wave vector $\mathbf{k}_f = (\tilde{k}_f, \tilde{k}_f, \tilde{k}_f)$. As an aside, let us recall that the Taylor-Green flow has a vanishing total helicity, e.g., $\int_{\mathcal{D}} \mathbf{u} \cdot (\nabla \times \mathbf{u}) = 0$.

3. Conventional definitions

We compute the isotropic energy spectrum as

$$E(k, t) := \frac{1}{2} \sum_{\mathbf{k}: k - \frac{1}{2} < |\mathbf{k}| \leq k + \frac{1}{2}} |\hat{\mathbf{u}}(\mathbf{k}, t)|^2,$$

from which both the (total) energy $E := \sum_{k=1}^{k_{\max}} E(k, t)$ and the enstrophy $\Omega := \sum_{k=1}^{k_{\max}} k^2 E(k, t)$ are estimated.

The nonlinear energy fluxes are defined through

$$\Pi(k, t) = \sum_{|\mathbf{k}| \geq k} T(\mathbf{k}, t), \quad \text{where}$$

$$T(\mathbf{k}, t) := \text{Re} \left\{ \sum_{i, j=1, 2, 3} \hat{u}_i^*[\mathbf{k}, t] \mathbb{P}_{i,j}(\mathbf{k}) [\mathbf{u} \times (\widehat{\nabla \times \mathbf{u}})]_j[\mathbf{k}, t] \right\}$$

represents the energy transfer function.

TABLE I. The three sets of runs discussed in this work.

Set	N_c	k_{\max}	E_0	f_0
A ₆₄	64	21.3	From 0.06 to 2.2	0.13
A ₁₂₈	128	42.6	From 0.06 to 2.2	0.12
B ₁₂₈	128	42.6	0.12	From 0.012 to 0.12

We finally define the forcing timescale as $\tau = \ell_f / \sqrt{E_0}$, with E_0 denoting either the prescribed RNS energy or a suitable time-averaged NS energy. Please observe that in Fourier space, the reversible viscosity defined in Eq. (3) is computed as

$$v_r[\mathbf{u}] = \epsilon_{\text{inj}} / \Omega \quad \text{with } \Omega \text{ the enstrophy,}$$

$$\text{and } \epsilon_{\text{inj}} := \text{Re} \left\{ \sum_{\substack{\mathbf{k}: |\mathbf{k}| \leq k_{\max} \\ i=1, 2, 3}} f_i(\mathbf{k}, t) \cdot u_i^*(\mathbf{k}, t) \right\} \quad (6)$$

representing the injected power due to the external forcing.

4. Parameters of the simulations

In order to carry a systematic investigation of the RNS system at fixed N_c and fixed forcing wave number $k_f = \sqrt{3}$, we follow two protocols, either (A) vary u_0 so that the runs have different E_0 for fixed f_0 ; or (B) vary f_0 using the same prescribed initial velocity amplitude $u_0 = 1$ (in which case all the corresponding RNS runs have the same total energy). Our discussion is based on three sets of runs of resolution up to 128^3 , the details and labels of which are summarized in Table I.

B. Results

We now present the outcome of our sets of numerical integrations of the RNS dynamics. We show that the characterization of the different statistical steady RNS states can be identified by tracing the time-averaged behavior of either the enstrophy or the reversible viscosity, depending on the control parameter \mathcal{R}_r . Those quantities stand out as relevant order parameters, that clearly demarcate the phase diagram in two regions $\mathcal{R}_r < \mathcal{R}_r^- \simeq 2$ and $\mathcal{R}_r > \mathcal{R}_r^+ \simeq 3.2$, in accordance with the two asymptotic states $\mathcal{R}_r \rightarrow 0$ and $\mathcal{R}_r \rightarrow \infty$. Both regimes have clear spectral signatures. We refer to the low- \mathcal{R}_r regime as being a *warm* statistical regime as it proves to be characterized by partial ultraviolet thermalization and therefore sensitive to the cutoff wave number k_{\max} . The high- \mathcal{R}_r regime apparently proves blind to this nonphysical artifactory cutoff, and we hence refer to the corresponding states as being of *hydrodynamic* type. The range $\mathcal{R}_r^- \leq \mathcal{R}_r \leq \mathcal{R}_r^+$ is a crossover region between those two regimes, over which both order parameters smoothly transit from being nearly vanishing to having finite positive values. This transition region is further characterized by the presence of strong bursts in the enstrophy times series, whose origin we tie to a nontrivial ultraviolet multistable behavior.

1. Statistical states of the RNS system

The enstrophy Ω is a quantity that naturally ties to small-scale structures and as such it is particularly sensitive even to early onsets of ultraviolet thermalization. For our purpose, it proves convenient to normalize the enstrophy as $\tilde{\Omega} := \Omega / \Omega_{\text{eq}}$, using the equilibrium value $\Omega_{\text{eq}} = 3k_{\max}^2 E_0 / 5$ (see Appendix for details).

Naturally, sensitivity to small scales is also monitored by the (nonsigned) reversible viscosity $v_r = \epsilon_{\text{inj}} / \Omega$. Averaging those values in time, one therefore naturally obtains two natural *order parameters*, which trace the different statistical regimes that the RNS system falls into. The asymptotic values of both parameters stems from the definition of \mathcal{R}_r . The fully thermalized asymptotics $\mathcal{R}_r \rightarrow 0$ has $\langle v_r \rangle \rightarrow 0$ and $\langle \tilde{\Omega} \rangle \rightarrow 1$, while the overdamped asymptotics $\mathcal{R}_r \rightarrow \infty$ corresponds to $\langle v_r \rangle \rightarrow \infty$ and $\langle \tilde{\Omega} \rangle \rightarrow 0$.

The values of $\langle v_r \rangle$ and $\langle \tilde{\Omega} \rangle$ for finite values of \mathcal{R}_r measured from our simulations are shown in Figs. 2(a) and 2(b), where the crudely depicted ‘‘crossover’’ of Fig. 1 between the large- \mathcal{R}_r *hydrodynamical* and the small- \mathcal{R}_r *thermalized* regimes can indeed be identified as the close vicinity of $\mathcal{R}_r^* = 2.75$.

This information can be refined by monitoring the dynamical behavior of the parameters, rather than their sole averaged values. To simplify the discussion, we choose to only comment on the time fluctuations of the normalized enstrophy, which we infer from Figs. 2(c) and 2(d). Specifically, Fig. 2(c) displays the dynamical evolution $\tilde{\Omega}$ for representative values of \mathcal{R}_r corresponding to the RNS set B₁₂₈, while Fig. 2(d) displays the time variance of $\tilde{\Omega}$ for every set of runs as a function of \mathcal{R}_r . Combining insights from both the averaged and the dynamical behaviors of $\tilde{\Omega}$, we then identify three ranges for the parameter \mathcal{R}_r , corresponding to the three types of RNS regimes hereafter described.

a. Hydrodynamic range. $\mathcal{R}_r > \mathcal{R}_r^+ \simeq 3.2$. In this range, the time-averaged reversible viscosities $\langle v_r \rangle$ reach finite positive values. The data collapse observed in Fig. 2(a) suggests that those values are prescribed by an increasing function of \mathcal{R}_r , independent from both the chosen protocol and the cutoff scale k_{\max} . This feature is compatible with the normalized enstrophy $\langle \tilde{\Omega} \rangle$ being nearly vanishing and behaving as a decreasing function of \mathcal{R}_r . Note that $\langle \tilde{\Omega} \rangle$ has some dependence on k_{\max} . This is evident from the observation that its profile for set A₆₄ in Fig. 2(b) lies above those for sets A₁₂₈ and B₁₂₈.

Furthermore, the enstrophy time series indicates that in this range of parameters, typical steady states have low fluctuations of the enstrophy. Empirical fits shown in Fig. 2(d) reveal that the normalized time variance of the enstrophies is reasonably well described as $[\text{Var}(\tilde{\Omega})]^{1/2} \simeq A_+ \langle \tilde{\Omega} \rangle / (\mathcal{R}_r / \mathcal{R}_r^* - 1)$, with $A_+ = 0.05$ and $\mathcal{R}_r^* = 2.75$, independently from k_{\max} .

b. Warm range. $\mathcal{R}_r < \mathcal{R}_r^- \simeq 2$. In this range of \mathcal{R}_r , the order parameters show some dependence on k_{\max} , as visible in Figs. 2(a) and 2(b). For the reversible viscosity, this can be accounted using Kubo dissipation theorem to estimate $\langle \epsilon_{\text{inj}} \rangle \sim f_0^2 \tau_{\text{eq}}$ in the limit $\mathcal{R}_r \rightarrow 0$. The timescale $\tau_{\text{eq}} \sim \ell_f E_0^{-1/2}$ is the *equilibrium* velocity correlation time at forcing scale, and is here prescribed by the fully thermalized statistics of truncated Euler flows [42,43]. Combining this estimate with the definitions (5) and (6), and using Eq. (A2) found in

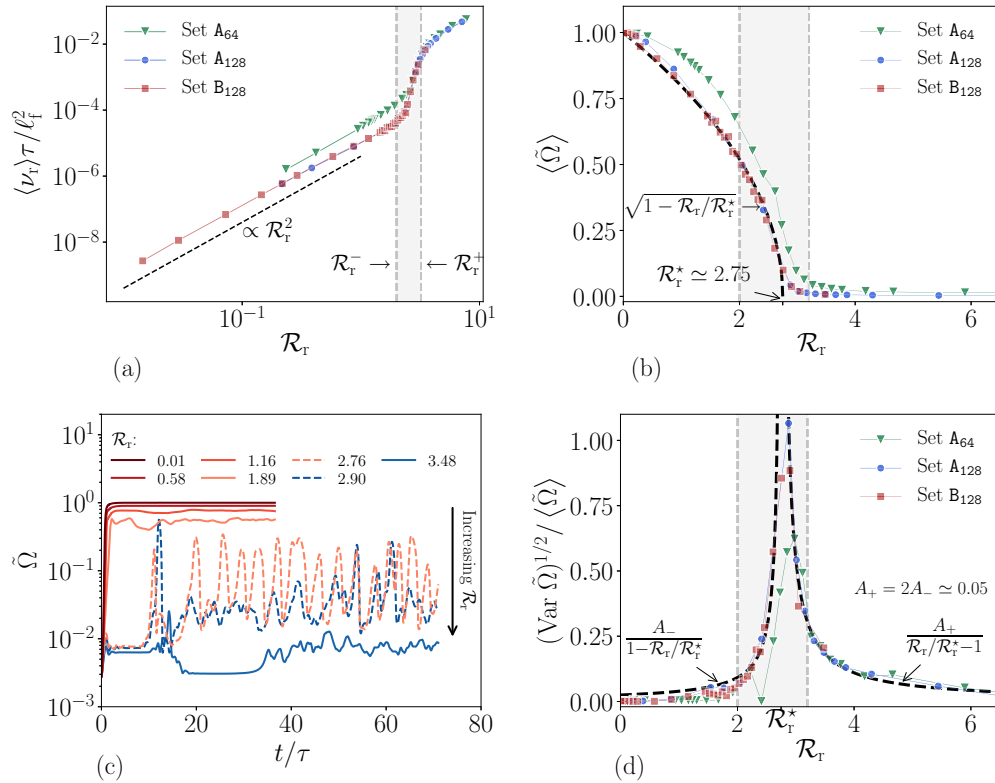


FIG. 2. Signatures of the RNS phase transition. (a) Time-average reversible viscosity ν_r vs \mathcal{R}_τ . Dotted lines represent the scaling $\nu_r \sim \mathcal{R}_\tau^2$, prescribed by the asymptotics $\mathcal{R}_\tau \rightarrow 0$ (see text for details). For $\mathcal{R}_\tau > \mathcal{R}_\tau^*$, the reversible viscosity becomes independent on the cutoff k_{\max} . This signals that the regime is of hydrodynamic type. (b) Time average of the normalized enstrophy $\tilde{\Omega}$ vs \mathcal{R}_τ , exhibiting a smooth transition in the vicinity of $\mathcal{R}_\tau^* \simeq 2.75$. $\tilde{\Omega} \in [0, 1]$ acts as an *order parameter*. (c) Time series of the normalized enstrophy ($\tilde{\Omega} := \Omega / \Omega_{\text{eq}}$) for representative values of the control parameter \mathcal{R}_τ from set B₁₂₈. (d) Time variance of $\tilde{\Omega}$ vs \mathcal{R}_τ showing the enhancement of the enstrophy fluctuations near $\mathcal{R}_\tau \sim \mathcal{R}_\tau^*$. In every figure, the gray-shaded area indicates a transition range delimited by $\mathcal{R}_\tau^- \simeq 2$ and $\mathcal{R}_\tau^+ \simeq 3.2$.

Appendix, one obtains

$$\langle \nu_r \rangle \sim \frac{\mathcal{R}_\tau^2 E_0^{3/2}}{\Omega_{\text{eq}} \ell_f} \propto \frac{\mathcal{R}_\tau^2}{k_{\max}^2} \text{ as } \mathcal{R}_\tau \rightarrow 0. \quad (7)$$

This asymptotics indeed accounts for the scaling behaviors observed in the numerics, which in fact extend through the entire warm range of \mathcal{R}_τ .

For the normalized enstrophy, the time average $\langle \tilde{\Omega} \rangle$ observed for the higher resolved sets of runs proves to be very accurately fitted by the square-root profile $\langle \tilde{\Omega} \rangle = (1 - \mathcal{R}_\tau / \mathcal{R}_\tau^*)^{1/2}$. The representative time series of Fig. 2(d) indicates that warm dynamics quickly reaches steady states characterized by vanishing levels of fluctuations for the enstrophy. As a function of \mathcal{R}_τ , those are fairly well described with the fit $[\text{Var}(\tilde{\Omega})]^{1/2} \simeq A_- \langle \tilde{\Omega} \rangle / (1 - \mathcal{R}_\tau / \mathcal{R}_\tau^*)$, with $A_- = 0.025$.

At the present stage, the specific shapes of the fitting profiles are to be considered as mere observations. Clearly, the fitting laws have mean-field flavors and hint toward unveiling a potential second-order phase transition. Yet, we postpone any further informed comments related to mean-field matters up until Sec. IV C 3, where similar behaviors will again appear but in a somewhat simplified setting, hence easier to insight from.

c. Transition range. $\mathcal{R}_\tau^- < \mathcal{R}_\tau < \mathcal{R}_\tau^+$. Within this narrow range of \mathcal{R}_τ , the order parameters sharply but *smoothly* transit

between their warm and their hydrodynamic behaviors: this precisely corresponds to the crossover region anticipated in Fig. 1. Let us observe that the critical value $\mathcal{R}_\tau^* \simeq 2.75$ previously obtained as a fitting parameter lies in that range. In fact, the mixed phase is essentially identified from the dynamical behavior of the enstrophy, which becomes bursty and characterized by successive peaks [cf. Fig. 2(c)]. Those do not eventually die out, and were found to remain up to the maximal integration time that we considered. The bursty behavior implies that the enstrophy fluctuations get drastically enhanced with respect to their the mean enstrophy values when approaching \mathcal{R}_τ^* from either the warm or the hydrodynamic side, and this is indeed the main signature of Fig. 2(d). At $\mathcal{R}_\tau = \mathcal{R}_\tau^*$, for example, we observe $[\text{Var}(\tilde{\Omega})]^{1/2} / \langle \tilde{\Omega} \rangle \sim 1$ for every set of runs, meaning that the time fluctuations are of the order of the time averages. Again, this behavior resembles a finite-size signature of a potential phase transition of finite order, that could perhaps appear in the limit of infinite resolution, that is to say, as $k_{\max} \rightarrow \infty$.

2. Spectral signatures of the RNS states

We here document the RNS energy spectra and fluxes observed in the different regimes, aiming at further characterizing the phase portrait of the RNS system *per se*, that is, without directly tying them to their NS counterpart or to

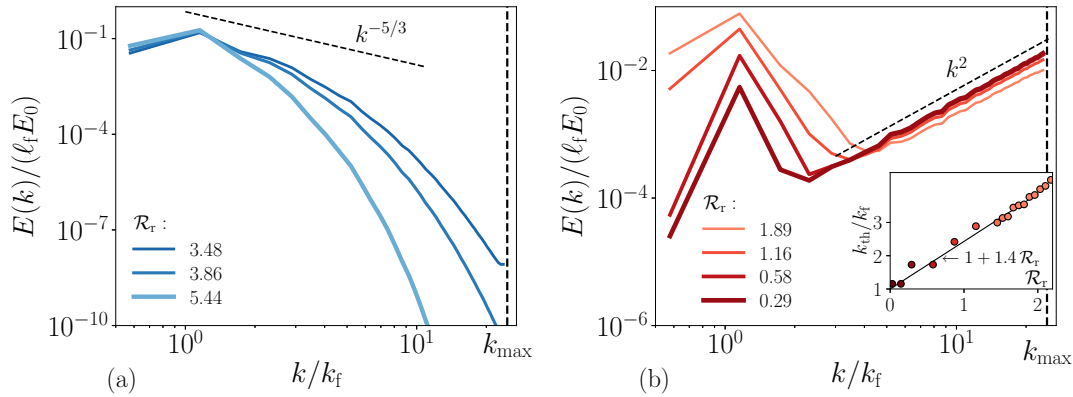


FIG. 3. Warm spectra vs hydrodynamic spectra. Main panels show the suitably normalized time-averaged energy spectra observed in the higher resolved RNS runs at $N_c = 128$ for various representative values of (a) $\mathcal{R}_r > \mathcal{R}_r^+$ corresponding to the hydrodynamic regime and (b) $\mathcal{R}_r < \mathcal{R}_r^-$ (from set B_{128}) corresponding to the warm regime. In the latter case, we observe an increasing range of wave numbers $k > k_{\text{th}}$ over which the spectra have Gibbsian scaling $E(k) \propto k^2$. k_{th} is defined as the wave number at which $E(k)$ is minimal. The inset reveals the affine dependence of k_{th} with \mathcal{R}_r , and suggests $k_{\text{th}} \rightarrow k_f \simeq 1$ as $\mathcal{R}_r \rightarrow 0$. The runs are taken from set A_{128} for $\mathcal{R}_r > 3.48$ and from set B_{128} otherwise.

the equivalence conjecture, at least for now. Let us recall that the RNS dissipative term relies on an intrinsic direct dynamical coupling with the forcing scale. It is therefore highly nonlocal in Fourier space, at sharp contrast with the standard NS viscous damping, which is local in k space. As such, the spectral signatures of the different RNS states are not obvious. *A priori*, it is unclear whether we should at all expect the RNS system to at least mimic standard NS *phenomenology* for prescribed ranges of \mathcal{R}_r .

a. Warm spectra vs hydrodynamic spectra. The analysis of Sec. III B 1 revealed that within the warm and the hydrodynamic phases, RNS dynamics reaches nonequilibrium steady states characterized by very low enstrophy fluctuations. In both of those phases, it is therefore natural to focus on time-averaged quantities. We define the (stationary) energy spectrum as the time average $E(k) := \langle E(k, t) \rangle$, where the angle brackets indicate an average over the total duration of the simulations. As shown in Fig. 3, both the warm and the hydrodynamical phases have clear spectral signatures, which naturally tie to the behavior of the order parameter studied in Sec. III B 1.

In the hydrodynamical phase, that is for $\mathcal{R}_r > \mathcal{R}_r^+$, the energy spectra have compact support in k space, as shown on Fig. 3(a). For $\mathcal{R}_r \gg \mathcal{R}_r^+$, the supports are narrow, the spectra being contained within a small- k range around the forcing scale. This means that the effective scale-by-scale damping mechanism generated from the reversible viscosity is large and dominates over the nonlinear transfer, somewhat akin to the standard laminar regime of textbook hydrodynamics. As \mathcal{R}_r decreases down to \mathcal{R}_r^+ , energy spreads toward the higher wave numbers $k > k_f$. The system is then in a nontrivial nonequilibrium steady state, with nonzero flux of energy, and multiscale statistics essentially independent from k_{max} : this could as well be taken as a heuristic defining statement of a turbulent state [44]! From this qualitative point of view, the RNS statistics observed at $\mathcal{R}_r = 3.48 \gtrsim \mathcal{R}_r^+$ do indeed describe turbulent motion.

At this stage though, the rather modest resolution of our numerics compared to current state-of-the-art NS simulations precludes us from drawing any conclusion as to whether

higher-resolved RNS simulations would indeed produce *fully developed turbulent statistics*, e.g., akin to those found in numerical and experimental data sets related to extreme regimes of fluid motion [45,46]. This issue precisely relates to Gallavotti's conjecture and we will discuss it in details in Sec. V A, in connection with a discussion on turbulent limits.

In the warm phase, here identified as $\mathcal{R}_r < \mathcal{R}_r^- \simeq 2$, the spectra are contaminated by the finite cutoff, as shown in Fig. 3(b). Specifically, they resemble some of the transients commonly observed in numerical simulations of the truncated Euler dynamics [37,38,47], in the sense that a seemingly infrared traditional hydrodynamic scaling at small k coexists with a nearly equilibrium ultraviolet power law scaling, that is $E(k) \sim k^\alpha$, where α progressively increases toward the Gibbs exponent $\alpha = 2$ as \mathcal{R}_r decreases toward 0. The separation between the two regions is identified in terms of a thermal wave number k_{th} , defined as the local minimum of the energy profile. The inset of Fig. 3(b) shows that as $\mathcal{R}_r \rightarrow 0$, k_{th} decreases linearly toward a value close to the forcing scale $k_{\text{th}} = \sqrt{3}$, e.g., close to the smallest wave number $k_0 = 1$. This is compatible with the fact that at $\mathcal{R}_r = 0$, the RNS steady state in fact corresponds to a fully thermalized *equilibrium* state of the truncated Euler equations, as previously explained in Sec. II B. Naturally, the approximate ultraviolet thermalization at $k > k_{\text{th}}$ accounts for the fact that the warm phase has a nonvanishing order parameter $\langle \tilde{\Omega} \rangle$, as indeed observed in Fig. 2, and explained with more technical details in the Appendix.

b. Energy spectra in the transition range. In the transition region, as evidenced by the violent fluctuations observed in the enstrophy time series, it is unclear whether the system genuinely reaches a steady state. It proves therefore more instructive to comment on the dynamics of the instantaneous energy spectra $E(k, t)$, rather than on their time-averaged values. In fact, the peaks observed in Fig. 2(c) clearly relate to oscillations of the ultraviolet behavior near k_{max} . Let us illustrate this by picking the RNS run of set B_{128} , corresponding to $\mathcal{R}_r = 2.76$, a value close to the identified critical point $\mathcal{R}_r^* = 2.75$ at which the fluctuations are the most enhanced. Figure 4(a) reports the dynamical evolution of the

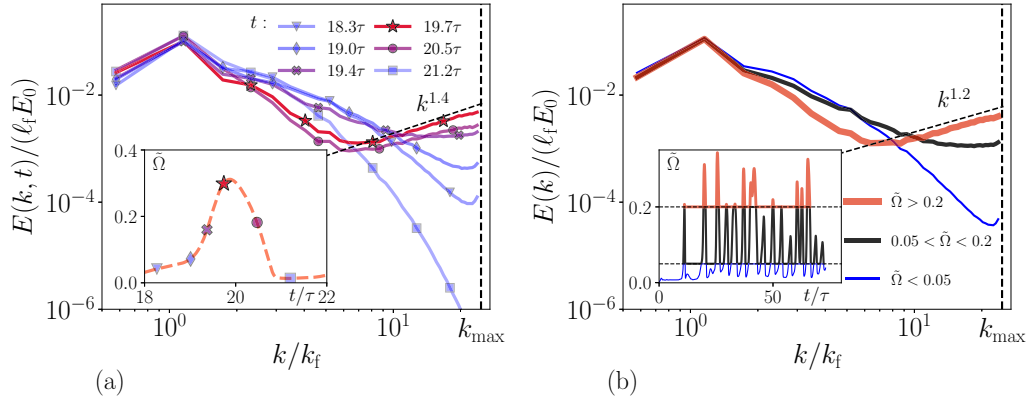


FIG. 4. Spectral multistability in the transition region $\mathcal{R}_r^- < \mathcal{R}_r < \mathcal{R}_r^+$. (a) Shows duly normalized *instantaneous* energy spectra from the RNS run $\mathcal{R}_r = 2.76$ of set B_{128} , observed at selected times, so as to trace one of the enstrophy burst revealed in Fig. 2(c). Inset zooms into the fluctuation time series. (b) Displays time averages of the energy spectra, conditioned on specific magnitudes of the normalized enstrophy, as specified by the inset.

energy spectra $E(k, t)$ on a short time interval $18\tau < t < 22\tau$, over which the normalized enstrophy abruptly varies from $\tilde{\Omega} \simeq 0.03$ at $t \simeq 18.3\tau$ to $\tilde{\Omega} \simeq 0.3$ at $t \simeq 19.7\tau$ back to $\tilde{\Omega} \simeq 0.01$ at $t = 21.2\tau$. Over this time interval, the infrared energy profile near the forcing scale remains essentially unchanged, but the ultraviolet profile drastically varies. It transits between being exponentially damped and being algebraic, with time-dependent scaling $E(k, t) \propto k^{\alpha(t)}$, over a scaling range whose size increases with the exponent α .

As the enstrophy increases in time toward its peak value, the exponent $\alpha(t)$ itself switches from negative to positive values, and the scaling range develops on a gradually increasing range. Let us observe that the maximum value reached by the scaling exponent is 1.4 and not 2, as would be expected if the system was partially thermalized.

It is an expected fact that enstrophy be particularly sensitive to small-scale behaviors. This is further illustrated in Fig. 4, where time averages of the energy spectra conditioned on prescribed enstrophy values are indeed observed to yield very different ultraviolet scaling ranges. For example, conditioning on $\tilde{\Omega} < 0.05$ yields a close-to-hydrodynamic type spectrum, while conditioning on the highest values $\tilde{\Omega} > 0.2$ produces ultraviolet scaling reminiscent of a warm Ω . Again, a closer inspection reveals that the relevant scaling exponent is only 1.2 and not 2.

This implies that while a finite k_{\max} indeed produces nonzero values for the order parameter $\langle \tilde{\Omega} \rangle$, the latter should vanish in the limit $k_{\max} \rightarrow \infty$. This naturally hints that the crossover range should disappear in that limit. This would imply $\mathcal{R}_r^- = \mathcal{R}_r^+ = \mathcal{R}_r^*$ asymptotically, and strongly suggests that the transition between the warm states and the hydrodynamics states become a genuine finite-order phase transition in the limit $k_{\max} \rightarrow \infty$.

c. Energy fluxes. In order to conclude our overview of the RNS states, let us briefly comment on the RNS energy fluxes, whose profiles for set B_{128} are represented in Fig. 5, in which they are normalized by the time-averaged injected power $\langle \epsilon_{\text{inj}} \rangle$. The transition from the hydrodynamic to the warm regime is reflected by the k -space profiles of the time-averaged fluxes $\Pi(k) := \langle \Pi(k, t) \rangle$, as shown in Fig. 5(a).

The flux profiles observed within the hydrodynamic range clearly mirror the energy spectra observations of Sec. III B 2 a. For large $\mathcal{R}_r > \mathcal{R}_r^+$, fluxes are indeed nonzero only in a small range of wave numbers $k \gtrsim k_f$. As \mathcal{R}_r decreases down to \mathcal{R}_r^+ , the spectral extension of the fluxes increases. For example, at $\mathcal{R}_r \approx 3.48$, where the energy spectra suggest that RNS dynamics is multiscale, we observe an energy flux that is significant up to $k \approx 10k_f$; this is in qualitative agreement with standard NS phenomenology at low Reynolds number. In particular, there is here no signature on the fluxes that the reversible dissipation is defined as a nonlocal operator in k space.

Within the warm range $\mathcal{R}_r < \mathcal{R}_r^-$, the fluxes follow a universal profile, that is seemingly independent of the specific value of \mathcal{R}_r , as indicated by the data collapse observed for $0.58 \lesssim \mathcal{R}_r \lesssim 1.89$. This is a clear signature of the warm statistical regime, yet also perhaps counterintuitive.

On the one hand, and except from their abrupt fall down to zero at the ultraviolet end, the fluxes are mostly constant over the entire k range above the forcing scale, e.g., here $2k_f \lesssim k \lesssim 20k_f$; this signals an out-of-equilibrium state, that should imply Kolmogorov scaling for the spectra. On the other hand, the corresponding energy spectra do not show this Kolmogorov spectra: Fig. 3(b) indicates close-to-equilibrium statistics, with a “distance” toward full thermalization monitored by the scale k_{th} becoming arbitrarily close to 1 as $\mathcal{R}_r \rightarrow 0$. This gradual convergence toward the equipartition state is not reflected by the flux profiles.

A qualitative explanation could be that the energy flux is an integrated quantity (see Sec. III A 3). Hence, if the range $k > k_{\text{th}}$ is indeed nearly thermalized and prescribed by equipartition statistics, then the latter do not contribute to the flux. An impatient and puzzled reader can, however, jump to the discussion of Eq. (16) at the end of Sec. IV C 1 to find that this kind of profile is in fact fully compatible with near-equilibrium and partially thermalized statistics.

As an aside, let us here point out that in the “warmest range” $\mathcal{R}_r \lesssim 0.5$, which is here not shown, $\Pi(k)$ begins to fluctuate wildly from the ultraviolet end. The amplitude of the normalized fluctuation grows with decreasing \mathcal{R}_r and destroys

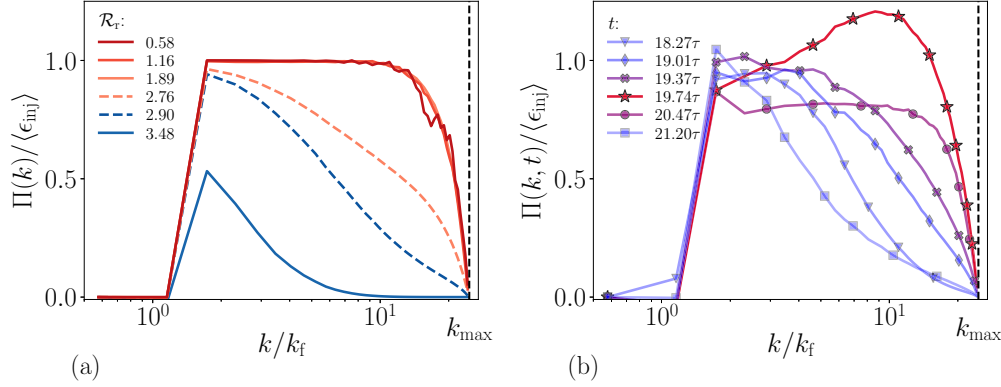


FIG. 5. RNS energy fluxes. Panels show the k -space profile of the energy fluxes $\Pi(k)$ normalized by the time-averaged injected power $\langle \epsilon \rangle_{\text{inj}}$, computed from set B₁₂₈, both (a) averaged over time for values of \mathcal{R}_τ representative of each RNS regime, and (b) for the $\mathcal{R}_\tau = 2.76$ run within the crossover region, at the same specific times considered in Fig. 4(a) tracing the enstrophy burst indicated in the corresponding inset.

the plateau behavior. The amplitude of the non-normalized $\Pi(k)$, however, correctly goes to zero and this is compatible with the truncated Euler limit with $E(k) \sim k^2$ across the full k range.

Within the transition range $\mathcal{R}_\tau^- < \mathcal{R}_\tau < \mathcal{R}_\tau^+$, Fig. 5 indicates that the large enstrophy fluctuations reflect in the fact that the instantaneous fluxes $\Pi(k, t)$ oscillate in time between a narrow-band hydrodynamic-type profile (at $t = 21.2\tau$ for example) and a zoology of full-band profiles, that for instance include the constant profile at $t = 20.5\tau$ or the nonmonotonic bumpy profile peaked at $k \simeq 10k_f$ in the vicinity of k_{max} at $t = 19.7\tau$, and corresponding to the local maximum monitored in the enstrophy time series.

IV. INSIGHTS FROM A REVERSIBLE LEITH-TYPE TOY MODEL

Our numerical analysis so far shows that the RNS system undergoes a continuous phase transition at \mathcal{R}_τ , whereby steady RNS solutions transit from being *hydrodynamic* to being *warm*, in the sense that their ultraviolet statistical features become affected by truncation scale and eventually thermalize. The smoothness of the transition is, however, a necessary consequence of our RNS runs having a finite resolution. While the behaviors of the order parameter of Fig. 2 strongly hint at the presence of a second-order transition with critical point $\mathcal{R}_\tau^* \simeq 2.75$, the numerical evidence is only suggestive: our runs have finite resolutions and this in principle precludes true divergence of any first derivative of the control parameter at the candidate critical point. For a similar reason, while we argued that the RNS equations at $\mathcal{R}_\tau \gtrsim \mathcal{R}_\tau^*$ produce multiscale steady states fitting a heuristic definition of “turbulence,” we are well aware that such a statement is only qualitative, due to the modest resolutions of our RNS runs. Consequently, it cannot provide a firm assessment regarding the validity of the equivalence conjecture. This is the reason why no quantitative comparison with NS runs has been commented on so far.

While runs at higher resolutions could be desirable, further insights on the nature of the transition can be obtained at smaller numerical cost from a simplified nonlinear diffusion spectral model of turbulence, namely, a modified Leith model of turbulent cascade [48], naturally tweaked to produce “re-

versible” statistics in the spirit of RNS dynamics. Such model proves simple to analyze because it has steady solutions that can be semianalytically determined, extending an approach previously used to characterize anomalous exponents found in the associated freely decaying dynamics [36,49–51]. As an aside, let us here point out that the terminology *warm solutions* used in this paper stems from the concept of *warm cascades* introduced by [36], which are explicit stationary solutions to the inviscid Leith model with simultaneous Kolmogorov infrared scaling and thermalized Gibbsian ultraviolet statistics.

Our analysis of the reversible Leith model suggests that its steady solutions indeed undergo a second-order phase transition, that separates hydrodynamic scaling from warm solutions. The transition is controlled by an order parameter \mathcal{R}_L akin to the RNS order parameter \mathcal{R}_τ , so that the phase diagram at finite value of k_{max} closely matches the one observed in the RNS simulations. The truncation scale k_{max} is found to play the role of (one over) a symmetry-breaking parameter, analogous to the magnetic field in statistical condensed matter. As such as $k_{\text{max}} \rightarrow \infty$, the system undergoes a genuine second-order phase transition, that is identified from a suitably defined susceptibility becoming infinite. We show that the statistical signatures of the phase transition can be captured from a heuristic mean-field Landau free energy. We conjecture that the picture extends to the RNS system, and this has practical implications regarding the equivalence conjecture.

A. Description of the reversible Leith model

The inviscid Leith model [36] consists in approximating dynamics of the energy spectrum in k space using a well-chosen second-order nonlinear diffusive operator. We here combine this nonlinear evolution for the energy profile $E(k, t)$ with a thermostat. The reversible Leith (RL) dynamics is then simply prescribed by

$$\frac{\partial E(k, t)}{\partial t} = -\frac{\partial \pi(k, t)}{\partial k} - \nu_L k^2 E(k, t),$$

$$\text{where } \pi(k, t) = -Ck^{11/2} E^{1/2}(k, t) \frac{\partial}{\partial k} \left[\frac{E(k, t)}{k^2} \right] \quad (8)$$

represents an energy flux and C is a dimensional constant that can be set to 1 for the sake of the present matter. The wave numbers k range from prescribed k_0 to the truncation wave number k_{\max} . In analogy with the RNS system, the parameter ν_L is to be interpreted as a reversible viscosity, that guarantees the time conservation of the total energy, that is

$$\int_{k_0}^{k_{\max}} E(k, t) dk = E_0 \text{ (prescribed)}. \quad (9)$$

We seek to characterize the nonequilibrium steady energy profiles $E(k)$ and associated flux $\pi(k)$, generated by the RL dynamics (8), when the following fluxes are prescribed at the boundaries:

$$\pi(k_0) = \epsilon_0 \text{ and } \pi(k_{\max}) = 0. \quad (10)$$

Combining the stationarity condition

$$-\frac{\partial \pi(k)}{\partial k} = \nu_L k^2 E(k), \quad (11)$$

with the boundary flux conditions (10), the reversible viscosity can be explicitly tied to the stationary energy profile $E(k)$ as

$$\nu_L = \frac{\epsilon_0}{\int_{k_0}^{k_{\max}} k^2 E(k) dk}. \quad (12)$$

The independent parameters that control the behavior of the steady energy profile are k_0 , k_{\max} , E_0 , together with the infrared boundary flux ϵ_0 . Letting $k_{\max} \rightarrow \infty$ and $\nu_L \rightarrow 0$ allows the possibility for nonvanishing constant flux solutions, characterized by the Kolmogorov scaling $E(k) \sim k^{-5/3}$. Such Kolmogorov solutions have finite capacity spectra, namely, $\int_{k_0}^{+\infty} E(k) dk < \infty$. In other words, the value of the total energy is independent from k_{\max} when $k_{\max} \rightarrow \infty$, and it is therefore natural to define a dimensionless number independent from k_{\max} , such as

$$\mathcal{R}_L = \epsilon_0^{2/3} \ell_0^{2/3} E_0^{-1}, \quad \text{with } \ell_0 = 2\pi/k_0. \quad (13)$$

The factor 2π entering the definition of the small scale ℓ_0 is purely cosmetic. Although it is defined in terms of a flux rather than in terms of a forcing intensity, the dimensionless number \mathcal{R}_L is the Leith analog of our previously defined \mathcal{R}_τ for the RNS system. It is the ratio between the injected energy at scale ℓ_0 and the total energy present in the system.

B. Construction of RL steady solutions

1. Grebenev parametrization

In order to construct steady solutions for the RL dynamics without resorting to direct numerical simulations of Eq. (8), we resort to the general strategy described in [51]. The general idea is to introduce a suitable parametrization (hereafter referred to as the ‘‘Grebenev parametrization’’) of the energy profile, that transforms the defining stationary condition (11) into an autonomous bidimensional dynamical system.

The specific form of the Grebenev parametrization is not particularly intuitive, but proves highly efficient. It consists in describing the steady energy profile using the change of

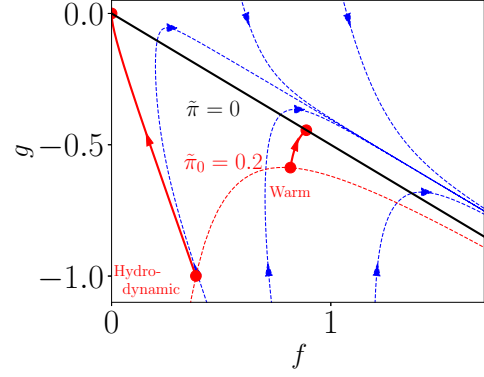


FIG. 6. Phase portrait of the dynamical system (15) obtained from the Grebenev parametrization of the Leith stationary profiles. Blue lines represent orbits and solid red lines are two examples of parametrizing trajectories with the same non-normalized infrared flux $\tilde{\pi}_0$. A warm solution with vanishing end-point energy flux follows a typical orbit up until the black line, while a scaling solution follows the single orbit that ends at $(0,0)$. Note that the two represented solutions have different k_{\max} .

variables $k, E(k), E'(k) \rightarrow \tau, f(\tau), g(\tau)$ defined through

$$\tau := \nu_L^{1/2} \int_{k_0}^k d\kappa (\kappa E(\kappa))^{-1/2},$$

$$f(\tau) := (E(k)\nu_L^{-1}k^{-1})^{1/2}, \text{ and } g(\tau) := f'/f - f. \quad (14)$$

In these variables, the stationary condition (11) transforms into the dynamical system

$$\begin{aligned} f'(\tau) &= f(f+g), \\ g'(\tau) &= -2(f+g)^2 - \frac{7}{2}f(f+g) + 2f^2 + \frac{1}{2}f. \end{aligned} \quad (15)$$

The system admits the stable fixed point $(0,0)$ and its phase portrait is shown in Fig. 6.

2. Practical use of the Grebenev parametrization

For a practical use of the Grebenev parametrization (14), it is convenient to work with the non-normalized energy spectra and fluxes, respectively defined as

$$\tilde{E}(k) := E(k)/\nu_L^2 = kf^2(\tau),$$

$$\text{and } \tilde{\pi}(k) := -\pi(k)/\nu_L^3 = k^4 f^2(f+2g).$$

For given k_0 and k_{\max} , we can then obtain RL steady solutions by integrating the system (15) from $\tau = 0$ with initial conditions f_0, g_0 until time τ_{\max} , implicitly defined from Eq. (14) as $\tau_{\max} = \int_{k_0}^{k_{\max}} dk/(kf(\tau))$. To construct the admissible solutions satisfying boundary conditions of type (10), we proceed in the following steps:

(1) Pick an initial value $\tilde{\pi}_0$ for the non-normalized flux at point k_0 . Initial admissible (f_0, g_0) are then such that $\tilde{\pi}_0 = k_0^4 f_0^2 (f_0 + 2g_0)$.

(2) Find (f_0, g_0) , such that $f(\tau_{\max}|f_0, g_0) + 2g(\tau_{\max}|f_0, g_0) = 0$. This ensures that $\pi(k_{\max}) = 0$ (up to some prescribed threshold).

(3) Compute $\nu_L = (\int_{k_0}^{k_{\max}} dk \tilde{E}(k))^{-1/2}$.

(4) Deduce $\epsilon_0 = \nu_L^3 \tilde{\pi}_0$.

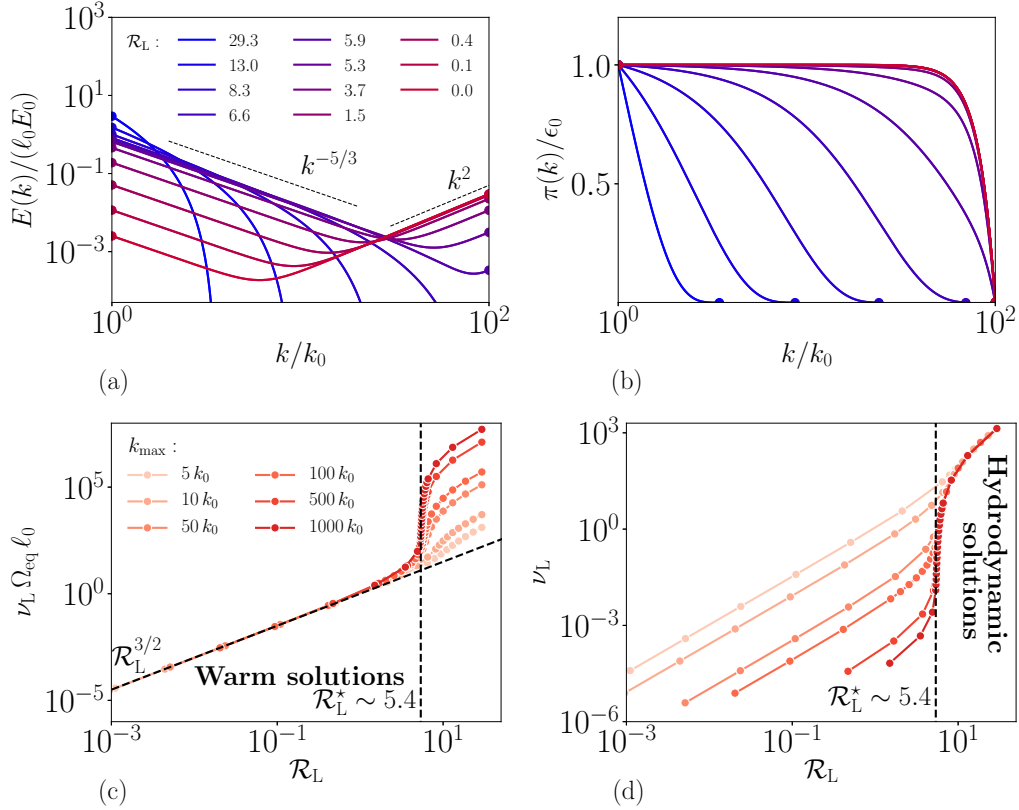


FIG. 7. Transition between warm and hydrodynamic states in the Leith model. Top panel shows the evolution of the steady profiles of (a) fluxes and (b) energies, for fixed values of $k_0 = 1/\ell_0 = 10^{-2}$ and $k_{\text{max}} = 1$. Above $\mathcal{R}_L^* \sim 5.4$, the energy spectra have compact support and exhibit inertial range Kolmogorov scaling as $\mathcal{R}_L \gtrsim 5.4$. Below \mathcal{R}_L^* , both Kolmogorov and equipartition scalings coexist: this is the warm regime. The corresponding energy fluxes are then constant throughout the scales and their normalized profile becomes independent of \mathcal{R}_L . Bottom panel shows the behavior of the RL viscosity as a function of \mathcal{R}_L for various choices of k_{max} , with (c) a suitable normalization illustrating the warm asymptotics $\nu_L \sim \mathcal{R}_L^{3/2}/\Omega_{\text{eq}} \ell_0$ or (d) without normalization, illustrating universality of the hydrodynamic regime with respect to k_{max} .

The resulting solution is a steady solution for the RL dynamics, with infrared flux ϵ_0 . Examples of trajectories in the (f, g) plane that parametrize either a hydrodynamic solution or a warm solution are represented in Fig. 6.

C. Transition between warm and hydrodynamical steady states

1. Qualitative overview

Using the Grebenev parametrization, we generate the RL steady energy and flux profiles for fixed $k_0 = 10^{-2}$, and various k_{max} ranging from $5k_0$ to $1000k_0$. For each pair (k_0, k_{max}) , we typically vary the non-normalized infrared flux $\tilde{\pi}_0$ from 10^{-10} to 10^{10} . The total energy E_0 is set to unity. We observe that at fixed k_0 and k_{max} , the steady RL solutions are uniquely determined by the value of the infrared-boundary flux ϵ_0 . The corresponding values of the reversible viscosity are then also uniquely determined.

Figure 7 provides a qualitative overview of the various RL statistical regimes generated by our algorithm, depending on the value of the reversible parameter \mathcal{R}_L . To comment on those, let us here use $k_0 = 10^{-2}$, $k_{\text{max}} = 1$ as a representative example. In Figs. 7(a) and 7(b) we show the profiles for the energy and corresponding stationary fluxes for various values of \mathcal{R}_L . It is apparent that the RL statistics exhibit a transition

somewhat akin to the one observed in RNS. Because of the broader range of scales, and probably because of the intrinsic simplicity of RL dynamics compared to RNS equations, clean scaling regimes here appear, which considerably refine the overall picture. In particular, the transition region is hardly visible and we do not identify its pertaining states.

Essentially, at large values of \mathcal{R}_L , the energy profile has compact support in k space and is therefore of hydrodynamic type. For $\mathcal{R}_L \simeq 29.3$, the highest value here represented, the energy spectrum $E(k)$ lacks any scaling region and is concentrated around the smallest wave number k_0 . Such is also the case for the energy flux: this corresponds to an overdamped regime, where the nonlinear terms prove unable to propagate the injected energy across the scales.

As \mathcal{R}_L decreases down to $\mathcal{R}_L \gtrsim 5.4$, the solutions develop Kolmogorov inertial ranges with $E(k) \sim k^{-5/3}$ over almost the full range of wave numbers. This feature goes along with the associated energy flux essentially becoming constant across an increasing range of wave numbers. Still, the energy profiles eventually drop down to zero at the highest wave numbers with an exponential rate. Let us remark that the development of a pure Kolmogorov scaling range in this hydrodynamic regime is less evident than it could seem at first thought: In particular, this contrasts with the anomalous

scaling solutions that typically appear in freely decaying infinite-range Leith models, whose infrared scaling exponents are known to be systematically larger than the constant-flux exponents [36,50].

Further decreasing \mathcal{R}_L below 5.4, the RL statistics sharply transit toward a warm regime. For $\mathcal{R}_L \lesssim 1.5$ down to 0, both Kolmogorov scaling $E(k) \sim k^{-5/3}$ and equipartition scaling $E(k) \sim k^2$ indeed coexist within the energy profile. As \mathcal{R}_L decreases down to 0, the equipartition scaling gradually invades the entire scaling range. We note that the warm energy fluxes are then nonvanishing and mostly constant over the range of wave numbers, regardless of the size of the equilibrium range. This exactly mimics the counterintuitive behavior observed in the RNS case and reported in Fig. 5.¹

In the Leith case, this puzzling but robust signature of the warm regime can, however, be accounted for. Let us first note that at fixed k_0 and E_0 , it stems from the definition of \mathcal{R}_L that $\epsilon_0 \rightarrow 0$ as $\mathcal{R}_L \rightarrow 0$. As such, while the normalisation used in Fig. 7(b) implies that the flux profile is constant in the \mathcal{R}_L regime, it should not misguide the reader into thinking that the flux is nonvanishing in the limit $\mathcal{R}_L \rightarrow 0$. This is not the case, and this nonanomalous feature is in due agreement with the statement that $\mathcal{R}_L \rightarrow 0$ corresponds to fully thermalized statistics. One can also remark that $\mathcal{R}_L \rightarrow 0$ also implies that $\nu_L \rightarrow 0$, as shown in Figs. 7(c) and 7(d).

The fact that the flux is constant across the scales is then a direct consequence of the stationarity condition (11), which reduces to $\partial_k \pi(k) = 0$ in the limit of vanishing reversible viscosity ν_L . Solving for the corresponding energy profiles up to an overall normalization constant, one obtains

$$E(k) \propto \left[5 \left(\frac{k}{k_{\text{th}}} \right)^3 + 6 \left(\frac{k}{k_{\text{th}}} \right)^{-5/2} \right]^{2/3}, \quad (16)$$

where k_{th} is the wave number at which $E(k)$ reaches its minimum and which depends on the initial conditions (ϵ_0, k_0) . It is readily checked that $E(k) \sim k^{-5/3}$ for $k \ll k_{\text{th}}$ and $E(k) \sim k^2$ for $k \gg k_{\text{th}}$: Eq. (16) provides an explicit example of a RL warm solution! There is therefore no contradiction in observing a constant flux simultaneously to a warm spectrum. Although the diffusion approximation is not valid in the RNS system, we believe that the property carries through for the RNS equations. While perhaps counterintuitive, the constant fluxes observed at low \mathcal{R}_r in Fig. 5 are fully compatible with the statement that the RNS statistics are warm in that regime.

2. Reversible viscosity and second-order phase transition

The previous description of the statistical regimes of RL dynamics at fixed values for (k_0, k_{max}) proves very generic and is mostly insensitive to the specific choice of k_{max} , at least provided that k_{max}/k_0 is taken sufficiently large. This can be directly inferred by monitoring the behavior of the reversible viscosity as a function of \mathcal{R}_L , which we represent in Figs. 7(c) and 7(d) for our various choices of k_{max} . The partitioning

between the warm and the hydrodynamic regimes appears clearly, and the transition value is to first order independent of k_{max} . The sharpening of the reversible viscosity profile as $k_{\text{max}} \rightarrow \infty$ suggests $\partial_{\mathcal{R}_L} \nu_L|_{\mathcal{R}_L=\mathcal{R}_L^*} \rightarrow \infty$ as $k_{\text{max}} \rightarrow \infty$, and suggests that the system undergoes a genuine phase transition at $\mathcal{R}_L = \mathcal{R}_L^* \simeq 5.4$. The observed continuity of the reversible viscosity at $\mathcal{R}_L \approx \mathcal{R}_L^*$ indicates the phase transition is continuous and of second order. The warm and the hydrodynamic regimes can therefore be identified as genuine *thermodynamic phases*.

In the warm phase $\mathcal{R}_L < \mathcal{R}_L^*$, the scaling behavior of ν_L for finite k_{max} is easily deduced from the definitions (12) and (13). As $\mathcal{R}_L \rightarrow 0$, one indeed obtains $\nu_L \sim \epsilon_0/\Omega_{\text{eq}} \sim (E_0 \mathcal{R}_L)^{3/2}/(\ell_0 \Omega_{\text{eq}})$, with Ω_{eq} denoting the value of the enstrophy when the energy spectrum is fully thermalized and $\propto k^2$. Figure 7(c) shows that the scaling in fact extends up until $\mathcal{R}_L \lesssim \mathcal{R}_L^*$. Please observe that the dependence of ν_L on the cutoff parameter through $\Omega_{\text{eq}} \propto k_{\text{max}}^2$ signals partial thermalization of the small scales, and implies that $\nu_L \rightarrow 0$ as $k_{\text{max}} \rightarrow \infty$.

In the hydrodynamic phase, by contrast, the reversible viscosity is independent of k_{max} as shown by Fig. 7(d). This reflects the fact that the statistics observed at finite $\nu_L > 0$ should be mostly independent of k_{max} as $k_{\text{max}} \rightarrow \infty$. Continuity of the reversible viscosity implies $\nu_L \rightarrow 0$ as $\mathcal{R}_L \gtrsim \mathcal{R}_L^*$.

3. A candidate mean-field Landau free energy

The interpretation of the RL “warm-hydro” transition in terms of a continuous transition can in fact be further substantiated and described in terms of a heuristic Landau theory (see, e.g., [52]) involving the parameters

$$\begin{aligned} r &:= \mathcal{R}_L/\mathcal{R}_L^* - 1 \quad (\text{“reduced temperature”}), \\ \mu &:= \tilde{\Omega}^{1/2} = (\Omega/\Omega_{\text{eq}})^{1/2} \quad (\text{“magnetization”}), \\ h &:= k_0/k_{\text{max}} \quad (\text{“magnetic field”}). \end{aligned} \quad (17)$$

Our choice of parameters is essentially data driven and motivated by successions of empirical tries. From Eq. (12), one can observe that the quantities ν_L and Ω^{-1} coincide in the steady state regime. As such, the order parameter μ could as well be defined from the reversible viscosity as $\mu \propto \nu_L^{-1/2}$ up to some appropriate normalization. This hydrodynamic magnetization is sensitive to ultraviolet thermalization and takes value 1 at $\mathcal{R}_L = 0$. In the hydrodynamic phase, it is nonvanishing for finite k_{max} , but converges to 0 as $k_{\text{max}} \rightarrow \infty$. This feature together with the fact that the transition is smooth for finite values of k_{max} is the main indication as to why (one over) k_{max} may be suitable as a smoothing symmetry-breaking parameter. Let us now consider the mean-field Landau free energy

$$\begin{aligned} \phi_L(\mu, h, r) &:= -3h\mu + \frac{1}{2}r^2\mu^2 + \frac{1}{4}\mu^4, \\ &\text{defined for } \mu \geq 0, h \geq 0, r \geq -1. \end{aligned} \quad (18)$$

The prefactor 3 in front of the symmetry-breaking term is data driven. In spite of its simplicity, Fig. 8 reveals that the mean-field free energy ϕ_L captures the essential signatures of the RL transition between the warm and the hydrodynamics phases.

¹The same feature is actually also observed in simulations of the truncated NS equations in the vanishing viscosity limit [56]. This result came to our knowledge during the final completion of this work.

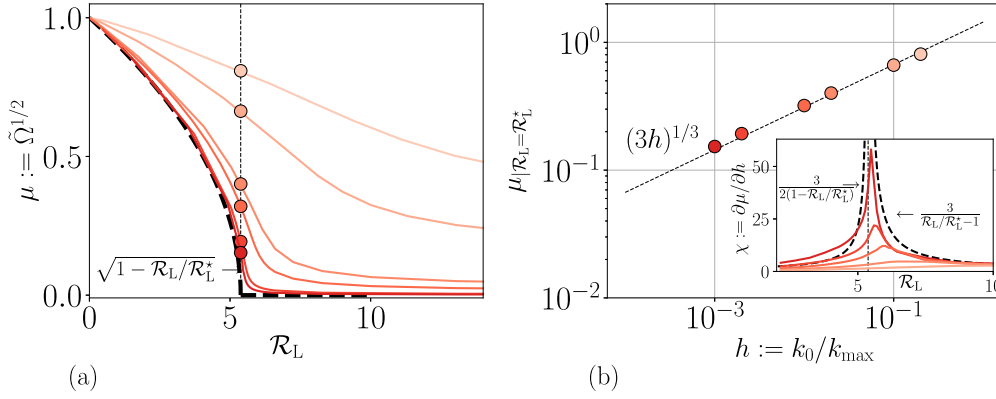


FIG. 8. Mean-field signatures of the RL transition. (a) Shows the spontaneous RL magnetization μ as a function of \mathcal{R}_r for $h = k_0/k_{\max}$ ranging from 0.2 to 0.001. The color scale is indicated by the dot colors in (b). In (b), the main figure shows the RL magnetization at critical point $\mu(r = 0, h)$ as a function of h . The inset shows the corresponding susceptibility $\chi(r, h)$ about the critical point estimated through finite differences. As such, no estimates are provided for $h = 0.2$. In every figure panel, the dashed lines indicate the mean-field predictions (19).

In particular, it predicts the following magnetization profiles:

$$\begin{aligned} \mu(r, h = 0^+) &= \sqrt{1-r} \quad \text{if } r > 0 \text{ and } 0 \text{ otherwise,} \\ \mu(r = 0, h) &= (3h)^{1/3}, \\ \chi(r, h) &:= \frac{\partial\mu}{\partial h} = \frac{3}{r} \quad \text{if } r > 0 \text{ and } \frac{3}{2r} \text{ otherwise.} \end{aligned} \quad (19)$$

Figure 8 shows that the first-order predictions for the magnetization are in excellent agreement with the RL data. The spontaneous magnetization $\mu(r, h)$ indeed seems to converge toward the mean-field prediction as h is decreased toward 0. At the critical point, the scaling with h is close to perfect over two decades. This rationally suggests that as $h \rightarrow 0$, the susceptibility $\chi(r = 0, h)$ indeed genuinely diverges, and that the RL transition is of second order. Deviations from our mean-field prediction seem to occur for the susceptibility. The mean-field exponent is compatible with the data, but a finer assessment would probably require reaching higher resolutions. We remark, that as predicted by (19), the behavior of $\chi(r, h)$ in the hydrodynamic phase is seemingly independent from h . Such is not the case in the warm case, and this is a deviation from our heuristic mean-field predictions.

Our partial conclusion at this point is that in spite of the warm second-order deviations from the mean field, Fig. 8 hints that the RL transition between warm and hydrodynamic states indeed fits into a general thermodynamic framework and corresponds to a second-order continuous phase transition. It is unclear whether specific properties of the transition could be deduced from first principles, but those considerations go beyond the scope of this work.

D. From reversible Leith to reversible Navier-Stokes dynamics

While the RL model has a very simple dynamics, it is naturally tempting to infer that the RNS statistics fits into a similar general thermodynamic framework as the one identified in the Leith case. We shall not refrain from doing so in Sec. V, in order to explore a thermodynamic formulation of Gallavotti's conjecture that could have practical implications for its rigorous numerical assessment. Prior to that, let us,

however, briefly point out at some salient differences between the RL and the RNS formulations.

a. \mathcal{R}_L vs \mathcal{R}_r . The specific definition of the reversible parameter differs between the RNS and the RL cases, due to the specific respective formulations of the reversible dynamics. As such, one should not expect the specific RL free energy (18) to account for the finite-size effects observed in our RNS numerics. Naturally, one could decide to investigate the RNS system in terms of a newly defined reversible parameter

$$\tilde{\mathcal{R}}_r := \langle \epsilon_{\text{inj}} \rangle^{2/3} \ell_r^{2/3} E_0^{-1}, \quad (20)$$

and this would provide an exact analog to the definition (13). Such a definition is natural, and would probably be the correct one to consider if one was to compare between different RNS forcing schemes. In fact, the only drawback of such a definition is that it relies on a data-driven measurement, namely, that of $\langle \epsilon_{\text{inj}} \rangle$. In this work, we see this only as a minor issue, with no relevance for the forthcoming discussion. In our view, this is one of the reasons why the RNS mean-field description does not, strictly speaking, carry through to the RNS statistics. However, upon defining the RNS hydrodynamic magnetization as $\mu_{\text{RNS}} := \tilde{\Omega}$ rather than the square-root RL definition (17), and upon using $r_{\text{RNS}} := \mathcal{R}_r/\mathcal{R}_r^* - 1$ as the RNS reduced temperature, it is apparent that the mean-field free energy prescribed by Eq. (18) correctly accounts for the phenomenological square-root fit of Fig. 2. One would require higher-resolved runs to analyze the RNS transition in terms of k_{\max} .

b. Dynamical behavior within the transition region. Another difference between the present RNS and RL formulations relates to the fact that the injected power fluctuates in time in the first case but not in the second case. We think that this feature prevents the RL dynamics to have a noticeable transition region at finite k_{\max} . Specifically in the Leith model, for a given input flux ϵ_0 and prescribed finite k_{\max} , only one steady solution exists. It is either a warm solution or a hydrodynamic solution: in other words, there is no multistability of solutions. This could as well be the case in the RNS system, if the injected power could be held constant in time. However, in our RNS formulation the injected power ϵ_{inj} is only constant on

average. In fact, it is unclear whether a forcing scheme could be implemented, that would inject energy at a constant rate in the RNS system without simultaneously breaking time reversibility. As such, insights from the Leith model necessarily relate to time averages rather than fluctuations. For example, at fixed total energy, the input parameter f_0 only imposes the upper bound: $|\epsilon_{\text{inj}}| \leq 2E_0|f_0|$. The enstrophy fluctuations observed in the transition region for the RNS simulations could therefore be simply due to power fluctuations, selecting either a warm solution or a hydrodynamic solution as a function of the instantaneous value of ϵ_{inj} . Those fluctuations therefore are not captured by the mean-field Landau description (17). Further intuitions on that matter could perhaps be obtained by generalizing the RL deterministic framework to a stochastic one, but again this goes beyond our present scope.

At any rate, and in spite of the intrinsic differences between the RNS and the RL formulations, it is natural to draw from the RL analysis, and interpret the RNS transition as a genuine second-order phase transition in the limit $k_{\text{max}} \rightarrow \infty$. This has practical implications for Gallavotti's conjecture, and those are substantiated in the next section.

V. TURBULENT LIMIT, CRITICAL POINT, AND GALLAVOTTI'S CONJECTURE

Our discussion has so far focused on the RNS statistics *per se*, that is, without reference to NS statistics, except for some very qualitative comments. Yet, as explained in the Introduction, the essential motivation in studying reversible dynamics in the first place is to assess whether Gallavotti's *equivalence conjecture* holds true. In essence, the conjecture states an identity between RNS and NS invariant measures, hereafter respectively written $\langle \cdot \rangle_{E_0}$ and $\langle \cdot \rangle_\nu$. Directly quoting from Ref. [33], we here state the equivalence as an (asymptotic) statistical identity valid for a suitable class of observable \mathcal{O} , e.g.,

$$\langle \mathcal{O} \rangle_\nu = \langle \mathcal{O} \rangle_{E_0} [1 + o(1)], \quad (21)$$

where $o(1)$ denotes a vanishing quantity in a suitable joint limit $\nu \rightarrow 0$, $k_{\text{max}} \rightarrow \infty$.² We shall not here attempt to further comment on the notion of a "suitable class of observables," except that the latter must contain the energy E , so that the following *reflexivity property* holds:

$$\langle E \rangle_\nu = E_0 [1 + o(1)]. \quad (22)$$

The notion of a "suitable joint limit" $\nu \rightarrow 0$, $k_{\text{max}} \rightarrow \infty$, however, needs further substantiation. In Ref. [33], the authors consider the limit $\nu \rightarrow 0$ at fixed value of k_{max} . This limit is particularly relevant in the perspective of the many interesting recent developments related to Galerkin-truncated dynamics [37,38,47,53–55]. In this limit, it is now known that the NS equations generate quasiequilibrium flows [56]. It is therefore not the relevant asymptotics in the context of describing fully

developed turbulence, which the (truncated) NS equations in principle generate in the joint ordered limit

$$k_{\text{max}} \rightarrow \infty \text{ first, } \nu \rightarrow 0 \text{ then,} \quad (23)$$

at fixed forcing statistics. Within the turbulent limit (23), the statistical identity (21) describes a candidate dynamical equivalence between the *full* RNS and the *full* NS statistics. To our understanding, this also corresponds to the original formulation of the equivalence conjecture [25,40].

Let us now explicitly assume that the RNS steady statistics are described by a second-order continuous phase transition at \mathcal{R}_r^* as $h := k_0/k_{\text{max}} \rightarrow 0$. One can then precisely identify the turbulent limit as the critical point asymptotics, approached from the hydrodynamic phase.

A. Turbulent limit and critical point asymptotics:

$$\mathcal{R}_r \rightarrow \mathcal{R}_r^* \text{ and } h \rightarrow 0$$

The identification of the turbulent limit as the critical point asymptotics is a consequence of the transition being continuous. Indeed, recalling the warm behavior $\langle \nu_r \rangle \propto h^2 \rightarrow 0$ illustrated in Figs. 2(a) and 7(c), we infer that the reversible viscosity is uniformly vanishing for $\mathcal{R}_r < \mathcal{R}_r^*$ in the limit $h \rightarrow 0$. Assumed continuity of the transition then yields $\langle \nu_r \rangle = 0$ at $\mathcal{R}_r = \mathcal{R}_r^*$. Besides, assuming say constant energy E_0 as $\mathcal{R}_r \rightarrow \mathcal{R}_r^*$, the forcing amplitude converges toward a finite limit, so that $f_0 \rightarrow f_0^* := \mathcal{R}_r^* E_0 / \ell_f$: We have recovered the turbulent limit (23).

Let us here comment on two salient features of this thermodynamic reformulation of a candidate RNS turbulent limit.

a. Order of the limits. In the limit $h \rightarrow 0$, the warm states are strictly speaking ill defined as a consequence of the ultraviolet catastrophe, as partially explained in Appendix. Hence, approaching the critical point from below necessarily requires taking the limit $\mathcal{R}_r \xrightarrow{\leftarrow} \mathcal{R}_r^*$ before $h \rightarrow 0$. By contrast, the hydrodynamic states are well defined even as $h \rightarrow 0$: We have extensively argued throughout our exposition that the statistics are independent from the cutoff in this phase. We therefore conjecture that approaching the critical point from above can therefore also be done by taking the thermodynamic limit *before* the critical limit: in other words, the limits $h \xrightarrow{\rightarrow} 0$, and $\mathcal{R}_r \xrightarrow{\rightarrow} \mathcal{R}_r^*$ should in principle commute. We can therefore unambiguously refer to the (unordered) joint limit $h \xrightarrow{\rightarrow} 0$, $\mathcal{R}_r \xrightarrow{\rightarrow} \mathcal{R}_r^*$ as the "turbulent limit."

b. Anomalous dissipation. In the limit $h \xrightarrow{\rightarrow} 0$, $\mathcal{R}_r \xrightarrow{\rightarrow} \mathcal{R}_r^*$, we could in principle expect anomalous dissipation from the RNS statistics. This is yet better seen if the alternative definition $\tilde{\mathcal{R}}_r$ of Eq. (20) indeed could be used as a valid reversible order parameter. One would then obtain $\langle \epsilon_{\text{inj}} \rangle \rightarrow \epsilon^* := \ell_f E_0^{3/2} \tilde{\mathcal{R}}_r^{3/2} < \infty$. This argument hints that scale-by-scale energy budget and associated $\frac{4}{5}$ laws could be deduced following the exact same steps as for the standard NS equations [13], hinting at the equivalence between those two dynamics at the critical point.

B. RNS vs NS near criticality: Illustrative numerics

As a final illustration of the relevance of the joint limit $k_{\text{max}} \rightarrow \infty$, $\mathcal{R}_r \xrightarrow{\rightarrow} \mathcal{R}_r^*$, let us here explicitly compare the

²Asymptotic statistical identities such as (21) are exactly the kind involved in modern treatments of the equivalence between the canonical and the microcanonical statistical ensembles, known to be valid for a wide class of systems in equilibrium statistical mechanics (see, e.g., [57] and references therein).

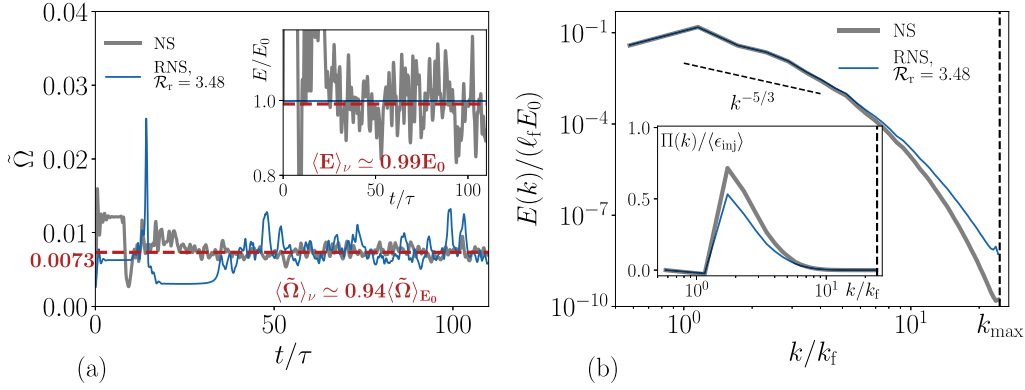


FIG. 9. RNS vs NS at $\mathcal{R}_\tau \gtrsim \mathcal{R}_\tau^*$. (a) Superimposes the times series of the normalized enstrophy (main panel) for the B_{128} RNS run at $\mathcal{R}_\tau = 3.48$ and a corresponding NS run, with same Taylor-Green forcing and standard viscosity set to $\nu = \langle \nu \rangle$. Inset shows the corresponding data for the energy time series, showing the approximated validity of the reflexivity property (see text). The dashed red lines indicate NS time averages. (b) Compares the time-averaged energy spectra (main panel) and fluxes (inset) for both the RNS and NS runs. Kolmogorov scaling is candidly indicated. E_0 is the conserved total energy of the RNS run.

RNS statistics from set B_{128} to their NS counterpart at $\mathcal{R}_\tau \sim 3.48 > \mathcal{R}_\tau^*$, a value which corresponds to the lower end of the hydrodynamic regime for our resolution. As previously stated, the RNS system then produces a nontrivial statistical state, which involves a multitude of length scales and timescales. To generate corresponding NS steady states, we integrate the NS equations with the same Taylor-Green forcing f_0 and standard viscosity set to $\nu = \langle \nu \rangle$. The main results are summarized in Fig. 9. The inset of Fig. 9(a) shows that the NS energy fluctuates around the imposed RNS value, e.g., $\langle E \rangle_\nu \simeq 0.99 E_0$, and this reflects the approximate validity of the reflexivity condition prescribed by Eq. (22). The main panel shows that the NS and the RNS enstrophy time series fluctuate around a similar mean value. The fluctuations are commensurate to each other, yet slightly larger for the RNS run.

Figure 9(b) shows that the RNS and the NS dynamics in that regime have in fact similar large-scale features. In particular, both the spectra and the fluxes show excellent agreement up to a decade ($k < 10 k_f$) before deviating in the ultraviolet range $k > 10 k_f$. This is a consequence of our simulations having finite resolution, and those would probably disappear upon taking larger k_{\max} for same f_0 , along with the expected decrease for the enstrophy fluctuations.

VI. CONCLUDING REMARKS

Time-reversible formulations of forced-dissipative hydrodynamical equations, addressing Gallavotti's equivalence conjecture of (hydro)dynamical ensembles, have emerged in recent years as an important candidate framework to provide an out-of-equilibrium thermodynamic perspective on the issue of turbulent irreversibility. Yet, in spite of many promising recent numerical results using reduced models, circumstances under which the equivalence conjecture might hold true remain unclear. As such, attention has recently shifted into analyzing reversible models where thermostats may preserve various quadratic quantities, and not necessarily the energy. In that context, the equivalence of ensemble has been assessed in the near equilibrium regime, corresponding to taking the vanishing viscosity at finite resolution [33–35].

In this work, we have followed a completely different route, in order to provide intuition on the potential validity of the equivalence conjecture for the full 3D dynamics, in the limit $k_{\max} \rightarrow \infty$, $\nu \rightarrow 0$. To that end, our analysis has focused on studying a reversible dynamics which preserves the kinetic energy. This defined the RNS dynamics. Rather than a systematic comparison of RNS statistics to NS statistics, we have carried out an extensive numerical study to fully explore the statistical regimes of the RNS system *per se*. To our knowledge, this approach reverses the philosophy of most of the previous numerical work related to Gallavotti's conjecture, and proved particularly insightful.

To summarize our results, our numerics hint that the RNS system undergoes a phase transition controlled by a non-negative dimensionless control parameter \mathcal{R}_τ , which quantifies the balance between the fluctuation of kinetic energy at the forcing length scale ℓ_f and the total energy E_0 .

For the presentation of our numerics, we explicitly used the definition $\mathcal{R}_\tau = f_0 \ell_f / E_0$, with f_0 parametrizing the forcing amplitude. We believe that alternative control parameters could as well be used that would not alter the overall picture, an example of which includes the data-driven $\tilde{\mathcal{R}}_\tau = \langle \epsilon_{inj} \rangle^{2/3} \ell_f^{2/3} / E_0$, with $\langle \epsilon_{inj} \rangle$ the stationary value of the injected power.

For small \mathcal{R}_τ , the RNS equations produce *warm* stationary statistics, e.g., characterized by the partial thermalization of the small scales and an intrinsic dependence on the cutoff k_{\max} . For large \mathcal{R}_τ , the stationary solutions have a hydrodynamic behavior, characterized by compact energy support in k space. The statistics are then essentially insensitive to the truncation scale k_{\max} .

The transition between the two statistical regimes was observed to be smooth but delimited within a narrow range of \mathcal{R}_τ in the vicinity of $\mathcal{R}_\tau^* \simeq 2.75$. It is characterized by a highly bursty dynamical behavior for the enstrophy, which is then found to fluctuate commensurately to its mean. In this regime, the system exhibits apparent multistability: it oscillates between a hydrodynamic-type low-enstrophy regime and a high-enstrophy regime, whose small-scale statistics are yet far from being thermalized and exhibit nontrivial power law

scalings. The enhancement of the enstrophy fluctuations in this transition region hints toward a second-order phase transition between the warm regime and the hydrodynamic regime, that would in a strict sense occur in the limit $k_{\max} \rightarrow \infty$, with both the time-averaged reversible viscosity and the time-averaged (normalized) enstrophy emerging as two natural order parameters. In our view, the smoothness of the transition is then a necessary consequence of the finite resolution of our numerics.

To substantiate this idea, we relied on a simple one-dimensional nonlinear ‘‘Leith-type’’ diffusion model, tweaked in such a way as to become a stylized energy-preserving reversible imitation of the RNS system. The main difference between such a reversible Leith dynamics (RL) and the RNS system is the forcing scheme, which in the previous case is imposed by requiring constant energy fluxes at the boundaries. Within this formulation, the RL steady states can be computed without relying on direct numerical integrations of the RL dynamics, but rather using a nontrivial parametrization and ideas from the theory of dynamical systems. Similarly to the RNS analysis, the RL steady regimes were classified depending on a dimensionless control parameter \mathcal{R}_L akin to \mathcal{R}_r and mimic the smooth transition between warm states and hydrodynamics states observed in RNS.

The simplicity of the RL formulation allowed us to investigate in details the finite-size effects and related influence of the cutoff k_{\max} . This asymptotic analysis substantiated the idea of a second-order phase transition: In fact, we found that the signatures of the phase transition close to the critical point \mathcal{R}_r^* could essentially be deduced from a heuristic mean-field Landau free energy. In this picture, \mathcal{R}_r indeed behaves as a thermodynamic control parameter, e.g., a temperature, the relevant order parameter is defined in terms of a suitably normalized enstrophy, while the symmetry-breaking parameter h is identified as (one over) the cutoff scale k_{\max} .

Naturally, the RL dynamics only reproduces idealized features of the RNS transition and has some important differences with the RNS system. In the Leith model, the critical control parameter is exclusively identified from the properties of the average steady state, and therefore does not account for the dynamical signatures of the transition found in the RNS system, namely, the enhancement of enstrophy variance near the transition. Besides, the small-scale energy in the high-enstrophy region $\mathcal{R}_L < \mathcal{R}_L^*$ remains up until \mathcal{R}_L^* close to being exactly thermalized, $E(k) \sim k^2$. This is at contrast with the RNS observations, in which close to the critical value \mathcal{R}_r^* , the power-law exponents of the energy spectrum at small scales are observed to fluctuate and are bounded by 2. This signals a clear departure from Gibbsian equipartition in the RNS system, and this is not captured by the simplified model. In our view, those differences can for the most part be traced back to the fact that the injected energy fluctuates in the RNS system but is kept a constant in our formulation of the RL dynamics.

In spite of the differences, it is natural to conjecture that such a second-order transition also exists for the RNS dynamics, so that a candidate RNS phase diagram could for example be akin to the one sketched in Fig. 10. If such was indeed the case, one could formulate the turbulent limit in which

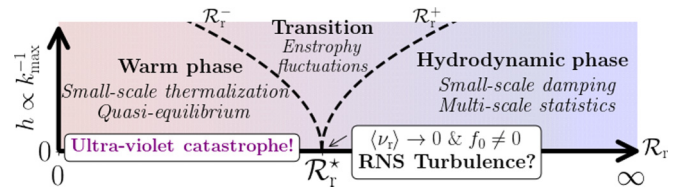


FIG. 10. A refined candidate phase diagram for the RNS steady state. Our numerical simulations suggest $\mathcal{R}_r^* \approx 2.75$.

one would ultimately desire to test Gallavotti’s conjecture in terms of the critical point asymptotics $\mathcal{R}_r \xrightarrow{\sim} \mathcal{R}_r^*$, $h \xrightarrow{\sim} 0$, with the overset symbol ‘‘ $\xrightarrow{\sim}$ ’’ indicating that those limits are approached from the hydrodynamic regime. In that limit, we have argued that the RNS states should have anomalous energy dissipation and formally vanishing thermostat, hinting at the validity of the equivalence conjecture. The suggestive comparison of RNS and NS numerics in that regime indeed hints toward the validity of this approach. Besides, we strongly believe that the limits $\mathcal{R}_r \xrightarrow{\sim} \mathcal{R}_r^*$ and $h \xrightarrow{\sim} 0$ should commute: Compared to standard formulation of the turbulent limit as $k_{\max} \rightarrow \infty$, $\nu \rightarrow 0$ in the NS equations, this would then constitute a major simplification, and hopefully paves the way to future systematic assessment of the equivalence conjecture.

In this work, we have indeed restricted ourselves both to numerical simulations involving rather modest numbers of grid points (up to $N_c^3 = 128^3$) and to statistical descriptions based on one point statistical quantities. The complete characterization of the statistical regimes of the RNS system with larger grid sizes is computationally very demanding, given that many of the runs require long temporal evolution. Yet, our results suggest to study the asymptotic behavior of RNS only at the transition, namely, by letting $N_c \rightarrow \infty$ at fixed $\mathcal{R}_r \gtrsim \mathcal{R}_r^*$. While we have provided evidence that in this regime the RNS system correctly reproduces the macroscopic properties of the NS equations, a systematic asymptotic analysis would at this point be desirable, to investigate the nature of the agreement at higher Reynolds number. Moreover, a careful investigation of more refined statistical properties beyond the relatively low-order statistics considered here is needed to complete the picture, but we leave it for future investigations.

ACKNOWLEDGMENTS

We thank Centre de Calcul Interactif, Université Nice Sophia Antipolis and Mésocentre de calcul intensif SIGAMM, Observatoire de la Côte d’Azur for computational resources. Part of this work was granted access to the following computing grants: GENCI (Grand Equipement National de Calcul Intensif) Grants No.: A0042A10441 (IDRIS and CINES), No. A0062A10441 (IDRIS, CINES and TGCC) and No. 2A310096 (IDRIS). B.D. acknowledges funding from ANR EXPLOIT, Grant Agreement No. ANR-16-CE06-0006-01. S.N. is supported by Chaire D’Excellence IDEX, Université de la Côte d’Azur, France. We thank G. Gallavotti and M. Cencini for their insightful remarks on preliminary versions of the paper.

APPENDIX: ABSOLUTE EQUILIBRIA OF THE TRUNCATED EULER EQUATIONS

For $\mathcal{R}_\tau = 0$, the numerical integration of the RNS equations exactly reduces to integrating the so-called “truncated Euler” equations. Those are in fact obtained by performing a Galerkin truncation of the full Euler dynamics at a maximum cutoff wave number k_{\max} . In practice, Galerkin truncations consist in suppressing all the triadic interactions involving wave numbers larger than k_{\max} , hereby yielding a high-dimensional conservative set of nonlinear ordinary differential equations. Truncated Euler flows exactly preserve the quadratic invariants of the original equations and satisfy a Liouville theorem. Hence, they typically converge toward thermal statistical states with Gibbsian statistics known as “absolute equilibria” [58–60], and the thermalization process usually exhibits interesting transients [37,38,47]. For the non-helical 3D truncated Euler flows that we consider in this paper, the relevant absolute equilibrium state is particularly simple and prescribed by each Fourier velocity mode having

independent centered Gaussian statistics with variance $\propto E_0/N_c^3$. This equilibrium state describes an equipartition of the total kinetic energy E_0 among the different modes. Assuming a continuous distribution of wave numbers, the corresponding energy spectrum can be estimated as

$$E_{\text{eq}}(k) = \frac{3E_0}{k_{\max}^3} k^2, \quad (\text{A1})$$

and the absolute equilibrium enstrophy is then

$$\Omega_{\text{eq}} := \int_1^{k_{\max}} k^2 E_{\text{eq}}(k) dk \underset{k_{\max} \rightarrow \infty}{\sim} \frac{3}{5} E_0 k_{\max}^2. \quad (\text{A2})$$

In the limit $k_{\max} \rightarrow \infty$, the absolute energy equilibria become ill defined, as the resulting energy spectra cannot be normalized, unless they are trivial and the total energy is vanishing. This phenomenon is the so-called “ultraviolet catastrophe,” which also prevents the warm RNS states to be properly defined in the limit $k_{\max} \rightarrow \infty$.

-
- [1] C. Cercignani, *The Boltzmann Equation and its Applications* (Springer, New York, 1988), pp. 40–103.
- [2] C. Cercignani, R. Illner, and M. Pulvirenti, *The Mathematical Theory of Dilute Gases*, Vol. 106 (Springer, New York, 2013).
- [3] S. Chibbaro, L. Rondoni, and A. Vulpiani, *Reductionism, Emergence and Levels of Reality, The Importance of Being Borderline* (Springer, Berlin, 2014).
- [4] R. Zwanzig, *J. Stat. Phys.* **9**, 215 (1973).
- [5] R. Zwanzig, *Nonequilibrium Statistical Mechanics* (Oxford University Press, Oxford, 2001).
- [6] B. Turkington, *J. Stat. Phys.* **152**, 569 (2013).
- [7] C. Gardiner, *Stochastic Methods*, Vol. 4 (Springer, Berlin, 2009).
- [8] L. Onsager and S. Machlup, *Phys. Rev.* **91**, 1505 (1953).
- [9] L. Bertini, A. De Sole, D. Gabrielli, G. Jona-Lasinio, and C. Landim, *J. Stat. Phys.* **107**, 635 (2002).
- [10] H. C. Öttinger, *Beyond Equilibrium Thermodynamics* (Wiley, Hoboken, NJ, 2005).
- [11] J. Kurchan, *J. Stat. Mech.: Theory Exp.* (2007) P07005.
- [12] R. Kraaij, A. Lazarescu, C. Maes, and M. Peletier, *J. Stat. Phys.* **170**, 492 (2018).
- [13] U. Frisch, *Turbulence: The Legacy of AN Kolmogorov* (Cambridge University Press, Cambridge, 1995).
- [14] J. Berg, B. Lüthi, J. Mann, and S. Ott, *Phys. Rev. E* **74**, 016304 (2006).
- [15] D. Buaria, B. Sawford, and P. Yeung, *Phys. Fluids* **27**, 105101 (2015).
- [16] D. Buaria, P. Yeung, and B. Sawford, *J. Fluid Mech.* **799**, 352 (2016).
- [17] S. S. Ray, *Phys. Rev. Fluids* **3**, 072601 (2018).
- [18] H. Xu, A. Pumir, G. Falkovich, E. Bodenschatz, M. Shats, H. Xia, N. Francois, and G. Boffetta, *Proc. Natl. Acad. Sci. USA* **111**, 7558 (2014).
- [19] H. Xu, A. Pumir, and E. Bodenschatz, *Sci. China Phys. Mech. Astron.* **59**, 614702 (2016).
- [20] A. Bhatnagar, A. Gupta, D. Mitra, and R. Pandit, *Phys. Rev. E* **97**, 033102 (2018).
- [21] A. Pumir, H. Xu, E. Bodenschatz, and R. Grauer, *Phys. Rev. Lett.* **116**, 124502 (2016).
- [22] J. Jucha, H. Xu, A. Pumir, and E. Bodenschatz, *Phys. Rev. Lett.* **113**, 054501 (2014).
- [23] K. P. Iyer, J. Schumacher, K. R. Sreenivasan, and P. Yeung, *Phys. Rev. Lett.* **121**, 264501 (2018).
- [24] Z.-S. She and E. Jackson, *Phys. Rev. Lett.* **70**, 1255 (1993).
- [25] G. Gallavotti, *Phys. Lett. A* **223**, 91 (1996).
- [26] G. Gallavotti and E. G. D. Cohen, *Phys. Rev. Lett.* **74**, 2694 (1995).
- [27] G. Gallavotti and E. G. D. Cohen, *J. Stat. Phys.* **80**, 931 (1995).
- [28] L. Biferale, D. Pierotti, and A. Vulpiani, *J. Phys. A: Math. Gen.* **31**, 21 (1998).
- [29] L. Rondoni and E. Segre, *Nonlinearity* **12**, 1471 (1999).
- [30] S. Aumaitre, S. Fauve, S. McNamara, and P. Poggi, *Eur. Phys. J. B* **19**, 449 (2001).
- [31] G. Gallavotti, L. Rondoni, and E. Segre, *Phys. D (Amsterdam)* **187**, 338 (2004).
- [32] S. Ciliberto and C. Laroche, *J. Phys. IV* **8**, Pr6 (1998).
- [33] L. Biferale, M. Cencini, M. De Pietro, G. Gallavotti, and V. Lucarini, *Phys. Rev. E* **98**, 012202 (2018).
- [34] G. Gallavotti (private communication).
- [35] M. De Pietro, L. Biferale, G. Boffetta, and M. Cencini, *Eur. Phys. J. E* **41**, 48 (2018).
- [36] C. Connaughton and S. Nazarenko, *Phys. Rev. Lett.* **92**, 044501 (2004).
- [37] C. Cichowlas, P. Bonaïti, F. Debbasch, and M. Brachet, *Phys. Rev. Lett.* **95**, 264502 (2005).
- [38] G. Krstulovic and M.-É. Brachet, *Phys. D (Amsterdam)* **237**, 2015 (2008).
- [39] S. Thalabard and B. Turkington, *J. Phys. A: Math. Theor.* **49**, 165502 (2016).
- [40] G. Gallavotti, *Phys. D (Amsterdam)* **105**, 163 (1997).
- [41] P. Debue, V. Shukla, D. Kuzzay, D. Faranda, E.-W. Saw, F. Daviaud, and B. Dubrulle, *Phys. Rev. E* **97**, 053101 (2018).
- [42] R. Kubo, *J. Phys. Soc. Jpn.* **12**, 570 (1957).

- [43] S. Thalabard and B. Turkington, *J. Phys. A: Math. Theor.* **50**, 175502 (2017).
- [44] G. Falkovich, in *Non-equilibrium Statistical Mechanics and Turbulence*, edited by S. Nazarenko and O. V. Zaboronski (Cambridge University Press, Cambridge, 2008), Chap. 1.
- [45] P. Yeung, X. Zhai, and K. R. Sreenivasan, *Proc. Natl. Acad. Sci. USA* **112**, 12633 (2015).
- [46] E.-W. Saw, D. Kuzzay, D. Faranda, A. Guittonneau, F. Daviaud, C. Wiertel-Gasquet, V. Padilla, and B. Dubrulle, *Nat. Commun.* **7**, 12466 (2016).
- [47] G. Krstulovic, P. D. Mininni, M. E. Brachet, and A. Pouquet, *Phys. Rev. E* **79**, 056304 (2009).
- [48] C. Leith, *Phys. Fluids* **10**, 1409 (1967).
- [49] C. Connaughton and R. McAdams, *Europhys. Lett.* **95**, 24005 (2011).
- [50] S. Thalabard, S. Nazarenko, S. Galtier, and S. Medvedev, *J. Phys. A: Math. Theor.* **48**, 285501 (2015).
- [51] V. N. Grebenev, A. Griffin, S. B. Medvedev, and S. V. Nazarenko, *J. Phys. A: Math. Theor.* **49**, 365501 (2016).
- [52] N. Goldenfeld, *Lectures on Phase Transitions and the Renormalization Group* (CRC Press, Boca Raton, FL, 2018).
- [53] R. H. Kraichnan, *Adv. Math.* **16**, 305 (1975).
- [54] U. Frisch, S. Kurien, R. Pandit, W. Pauls, S. S. Ray, A. Wirth, and J.-Z. Zhu, *Phys. Rev. Lett.* **101**, 144501 (2008).
- [55] S. S. Ray, *Pramana* **84**, 395 (2015).
- [56] A. Alexakis and M.-E. Brachet, [arXiv:1906.02721](https://arxiv.org/abs/1906.02721).
- [57] H. Touchette, *J. Stat. Phys.* **159**, 987 (2015).
- [58] T. Lee, *Q. Appl. Math.* **10**, 69 (1952).
- [59] R. H. Kraichnan, *Phys. Fluids* **10**, 1417 (1967).
- [60] R. H. Kraichnan, *J. Fluid Mech.* **59**, 745 (1973).